

AD-A185 270

DTIC FILE COPY

AD

12

TECHNICAL REPORT BRL-TR-2833

COMPUTATIONAL AERODYNAMIC
ANALYSIS FOR A RANGE-LIMITED
25mm TRAINING ROUND

BERNARD J. GUIDOS
WALTER B. STUREK

DTIC
ELECTE
OCT 07 1987
S D

AUGUST 1987

APPROVED FOR PUBLIC RELEASE; DISTRIBUTION UNLIMITED.

US ARMY BALLISTIC RESEARCH LABORATORY
ABERDEEN PROVING GROUND, MARYLAND

87 10 6 137

APR 185 270

REPORT DOCUMENTATION PAGE

Form Approved
OMB No 0704-0188
Exp Date Jun 30, 1986

1a. REPORT SECURITY CLASSIFICATION UNCLASSIFIED		1b. RESTRICTIVE MARKINGS	
2a. SECURITY CLASSIFICATION AUTHORITY		3. DISTRIBUTION / AVAILABILITY OF REPORT Approved for public release, distribution unlimited.	
2b. DECLASSIFICATION / DOWNGRADING SCHEDULE		4. PERFORMING ORGANIZATION REPORT NUMBER(S) BRL-TR-2833	
4. PERFORMING ORGANIZATION REPORT NUMBER(S)		5. MONITORING ORGANIZATION REPORT NUMBER(S)	
6a. NAME OF PERFORMING ORGANIZATION US Army Ballistic Research Laboratory	6b. OFFICE SYMBOL (if applicable) SLCBB-LF-R	7a. NAME OF MONITORING ORGANIZATION	
6c. ADDRESS (City, State, and ZIP Code) Aberdeen Proving Ground, Maryland 21005-5066		7b. ADDRESS (City, State, and ZIP Code)	
8a. NAME OF FUNDING / SPONSORING ORGANIZATION	8b. OFFICE SYMBOL (if applicable)	9. PROCUREMENT INSTRUMENT IDENTIFICATION NUMBER	
8c. ADDRESS (City, State, and ZIP Code)		10. SOURCE OF FUNDING NUMBERS	
		PROGRAM ELEMENT NO. 62618A	PROJECT NO. 1L162618AH80
		TASK NO.	WORK UNIT ACCESSION NO.
11. TITLE (Include Security Classification) COMPUTATIONAL AERODYNAMIC ANALYSIS FOR A RANGE-LIMITED 25MM TRAINING ROUND			
12. PERSONAL AUTHOR(S) R. J. Guidos and W. B. Stupak			
13a. TYPE OF REPORT Technical Report	13b. TIME COVERED FROM _____ TO _____	14. DATE OF REPORT (Year, Month, Day)	15. PAGE COUNT
16. SUPPLEMENTARY NOTATION			
17. COSATI CODES		18. SUBJECT TERMS (Continue on reverse if necessary and identify by block number)	
FIELD	GROUP	SUB-GROUP	
01	01	Computational Aerodynamics	
19	04	Parabolized Navier-Stokes	
		25mm Training Round	
		Aerodynamics Analysis	
		Supersonic Projectile	
		Spin-Stablized Shell	
19. ABSTRACT (Continue on reverse if necessary and identify by block number) A computational aerodynamics study is presented for an initial design configuration intended for use as a training round for a 25mm gun. The shell is designed with a non-axisymmetric boattail which induces a large de-spin moment. The purpose for such a design is to limit the range of the round through aerodynamic destabilization. The paper reports a computational aerodynamics study using a thin-layer Parabolized Navier-Stokes computational technique. Static aerodynamic coefficients and roll damping are computed for a range of supersonic Mach numbers and boattail lengths. Comparisons are made with computational predictions for axisymmetric configurations and firing range data. A six degree-of-freedom trajectory simulation code is used to estimate the early flight characteristics for the configurations of interest.			
20. DISTRIBUTION / AVAILABILITY OF ABSTRACT <input type="checkbox"/> UNCLASSIFIED/UNLIMITED <input type="checkbox"/> SAME AS RPT <input type="checkbox"/> DTIC USERS		21. ABSTRACT SECURITY CLASSIFICATION UNCLASSIFIED	
22a. NAME OF RESPONSIBLE INDIVIDUAL Ronald J. Guidos		22b. TELEPHONE (Include Area Code) (301) 278-5436	22c. OFFICE SYMBOL SLCBB-LF-R

18. SUBJECT TERMS (Continued)

Non-Axisymmetric Shell
Non-Conical Boattail

Roll Damping
Trajectory Simulation

TABLE OF CONTENTS

	<u>Page</u>
LIST OF FIGURES.....	v
I. INTRODUCTION.....	1
II. MODEL AND TEST CONDITIONS.....	1
III. COMPUTATIONAL APPROACH.....	2
1. GOVERNING EQUATIONS/NUMERICAL METHOD.....	2
2. INITIAL AND BOUNDARY CONDITIONS.....	3
3. QUASI-STEADY APPROXIMATION.....	3
IV. PRELIMINARY ANALYSIS.....	4
1. BACKGROUND.....	4
2. STATIC AERODYNAMIC ANALYSIS.....	5
V. RESULTS.....	7
1. ROLL DAMPING.....	8
2. PITCH-PLANE AERODYNAMICS.....	8
3. DRAG.....	9
4. ROLL ORIENTATION.....	9
5. TRAJECTORY SIMULATION.....	10
VI. CONCLUSIONS.....	12
REFERENCES.....	45
LIST OF SYMBOLS.....	47
DISTRIBUTION LIST.....	51



Accession For	
NTIS CRA&I	<input checked="" type="checkbox"/>
DTIC TAB	<input type="checkbox"/>
Unannounced	<input type="checkbox"/>
Justification	
By	
Distribution/	
Availability Codes	
Dist	Availability Special
A-1	

LIST OF FIGURES

<u>Figure</u>		<u>Page</u>
1	Non-axisymmetric shell configuration.....	16
2	Roll orientation and direction of spin looking upstream.....	17
3	Physical and computational grid coordinates and notation.....	18
4	Coordinate system/sign conventions for aerodynamic coefficients.....	19
5	Validation of quasi-steady assumption for roll damping, Mach = 5, $\alpha = 0^\circ$, non-axisymmetric configuration.....	20
6	Cross-sectional areas of triangular non-conical boattail and 7° conical boattail as functions of axial position.....	21
7	Roll damping developing over body, Mach = 5, $\alpha = 0^\circ$, axisymmetric and non-axisymmetric configurations.....	22
8	Roll damping developing over body, $\alpha = 0^\circ$, non-axisymmetric configuration.....	23
9	Roll damping of non-axisymmetric configuration with different boattail lengths, $\alpha = 0^\circ$	24
10	Roll damping of 1/2 caliber non-conical boattail configuration; comparison between computation and experiment.....	25
11	Normal force coefficient developing over body, Mach = 3, $\alpha = 2^\circ$, axisymmetric and non-axisymmetric configurations.....	26
12	Slope of normal force coefficient for non-axisymmetric configuration with different boattail lengths.....	27
13	Pitch-plane center of pressure for non-axisymmetric configuration with different boattail lengths.....	28
14	Linear pitching moment coefficient for non-axisymmetric configurations with different boattail lengths.....	29
15	Linear pitching moment coefficient for 1/2 caliber non-conical boattail configuration with small base cavity; comparison between computation and experiment.....	30
16	Linear pitching moment coefficient for axisymmetric and non-axisymmetric configurations with 1/2 caliber boattail.....	31
17	Linear pitching moment coefficient for axisymmetric and non-axisymmetric configurations with 1 caliber boattail.....	32

LIST OF FIGURES (Continued)

<u>Figure</u>		<u>Page</u>
18	Linear pitching moment coefficient for axisymmetric and non-axisymmetric configurations with 1-1/2 caliber boattail.....	33
19	Linear pitching moment coefficient for axisymmetric and non-axisymmetric configurations with 2 caliber boattail.....	34
20	Forebody drag coefficient developing over body, Mach = 1.5, $\alpha = 0^\circ$, axisymmetric and non-axisymmetric configurations.....	35
21	Forebody drag coefficient developing over body, Mach = 3, $\alpha = 0^\circ$, axisymmetric and non-axisymmetric configurations.....	36
22	Forebody drag coefficient for non-axisymmetric configuration with different boattail lengths, $\alpha = 0^\circ$	37
23	Base drag coefficient for non-axisymmetric configuration with different boattail lengths, $\alpha = 0^\circ$	38
24	Total drag coefficient for non-axisymmetric configuration with different boattail lengths, $\alpha = 0^\circ$	39
25	Total drag coefficient for 1/2 caliber non-conical boattail configuration; comparison between computation and experiment.....	40
26	Trajectory simulation for non-axisymmetric configurations; Mach number as a function of range.....	41
27	Trajectory simulation for non-axisymmetric configurations; yaw angle as a function of range.....	42
28	Trajectory simulation for non-axisymmetric configurations; nondimensional spin rate as a function of range.....	43
29	Trajectory simulation for non-axisymmetric configurations; gyroscopic stability as a function of range.....	44

I. INTRODUCTION

The ability to predict the aerodynamics of shell through the use of advanced computational methods is becoming an important factor in the design and testing of current and future systems of interest to the U.S. Army. State-of-the-art technology is being applied at BRL in a continuing research effort directed towards computing the aerodynamic forces that determine the behavior of shell. Through advanced finite-difference techniques which are being used to solve the thin-layer Navier-Stokes equations, improvements in computational predictive capabilities for shell are being achieved.

This paper documents a computational aerodynamics study of an initial design configuration which is intended for use as a training round for a 25mm gun. The design configuration of interest is similar to a standard spinning shell with one important difference: the boattail is beveled such that axisymmetry no longer exists about the projectile axis. Referred to as a non-conical boattail¹⁻² (NCBT), this geometric feature causes a large de-spin moment to act upon the spinning shell.

The non-conical boattail is expected to reduce the gyroscopic stability enough to cause the shell to become unstable in flight. Thus it is desirable to determine the roll damping of the shell as a function of both Mach number and boattail length. The overall predicted static aerodynamic behavior of this non-axisymmetric shell is presented. Comparisons are made with computational predictions for axisymmetric configurations as well as range firings.

The computational approach used in this study is the thin-layer Parabolized Navier-Stokes (PNS) technique reported by Schiff and Steger.³ This PNS technique has been used successfully to predict the steady, three-dimensional, viscous, supersonic flow for axisymmetric spinning shell at small angles of attack ($\alpha < 6^\circ$).⁴⁻⁶ This method has also been applied to non-axisymmetric configurations at zero spin with encouraging results.⁷

The PNS approach offers certain advantages over time-dependent solutions that are considered important for this study. Computer storage and CPU requirements are much less, making parametric studies over a range of Mach numbers and angles of attack more feasible. At the same time, it is of interest to apply the PNS technique to current problems that test its capabilities and define its limitations. This report describes computational results using the PNS technique for a configuration of non-axisymmetry applicable to spin rates typical of army gun twist.

II. MODEL AND TEST CONDITIONS

The shell configuration of interest is depicted in Figure 1. The shell consists of a 3 caliber secant-ogive nose and a .75 caliber cylindrical mid-section. The reference diameter of the body is 13.5 mm (sub-caliber round), occurring at the cylindrical midsection. The afterbody consists of a triangular non-conical boattail of lengths varying to a maximum of 2 calibers. The non-conical boattail is made up of three non-canted 7° beveled cuts spaced at 120° intervals around the body. The initial design configuration has a 1/2 caliber non-conical boattail.

The computational shell geometry possesses a sharp nosetip, whereas the actual shell geometry possesses a rounded nosetip with a bluntness ratio of 8%. Reference 5 indicates that such a small bluntness ratio has a negligible effect on the pitch-plane aerodynamics of shell. The blunt nosetip contribution to aerodynamic drag, however, is likely to be noticeable. In this study, differences in aerodynamic performance due to contributions from other than geometric non-axisymmetry are of minimal interest. For purposes of clarity, however, it should be noted that the sharp ogive nosetip is itself modeled by a small conical extension possessing a half-angle of 13.7°.

The dominant geometric feature of the shell of interest is the triangular non-conical boattail. Figure 1 shows the non-conical boattail consisting of three non-canted 7° beveled cuts spaced at 120° intervals around the body. Computations were also made for two axisymmetric configurations consisting of the same forebody as in Figure 1 but with 0° and 7° boattails. Computations were performed for boattail lengths varying from zero to 2 calibers. Figure 1 shows a full 2 caliber boattail; shorter boattail configurations were truncations of the full 2 caliber boattail. Figure 2 shows the convention for roll orientation for the non-axisymmetric shell.

The test conditions are sea-level atmospheric. The Mach numbers are 1.5, 3, and 5; the Reynolds numbers based on body diameter are $.458 \times 10^6$, $.917 \times 10^6$ and 1.52×10^6 respectively. Both the free stream static temperature and the body wall temperature are taken as 273K, and the boundary layer is assumed to be fully turbulent. The angle of attack is assumed to be in the linear range, from zero to 2°. For cases with spin, a non-dimensional spin rate of $PD/V = .1417$ corresponds to a gun twist of 23.94 calibers of transit per revolution for this sub-caliber round.

III. COMPUTATIONAL APPROACH

1. GOVERNING EQUATIONS/NUMERICAL METHOD

The results for this study were obtained using the thin-layer Parabolized Navier-Stokes (PNS) technique as formulated by Schiff and Steger.³ The PNS equations can be marched spatially along the body in the direction where the flow is supersonic and contains no streamwise separation. The thin-layer approximation⁸ retains the viscous derivatives in the radial direction only.

By employing the subsonic sublayer approximation as discussed in Reference 3, the steady, three-dimensional, thin-layer equations in strong conservative form can be written as:

$$\frac{\partial \hat{E}_s}{\partial \xi} + \frac{\partial \hat{F}}{\partial \eta} + \frac{\partial \hat{G}}{\partial \zeta} = \frac{1}{\hat{r}} \frac{\partial \hat{S}}{\partial \zeta} \quad (1)$$

where ξ, η, ζ are the fixed generalized coordinate variables shown in Figure 3, where:

$\xi = \xi(x)$ is the streamwise, longitudinal (marching) coordinate

$n = n(x,y,z)$ is the circumferential coordinate

$\zeta = \zeta(x,y,z)$ is the radial coordinate, with the body mapped onto the $\zeta = 0$ plane.

Equation (1) represents the thin-layer approximation to the equations of mass, momentum, and energy conservation in the three coordinate directions. The inviscid flux vectors \hat{E}_s , \hat{F} , \hat{G} and the thin-layer model viscous term \hat{S} are functions of the dependent variables represented by the vector \bar{q} , given by:

$$\bar{q}^T = (\rho, \rho u, \rho v, \rho w, e)$$

Equation (1) is solved by applying the conservative, approximately factored, implicit, delta form, finite-difference numerical algorithm formulated by Beam and Warming.⁹ A fully turbulent boundary layer is simulated using the two-layer algebraic model of Baldwin and Lomax.⁸

2. INITIAL AND BOUNDARY CONDITIONS

An initial cross-sectional plane of data is obtained near the nosetip of the projectile through the use of a step-back procedure which employs the conical flow assumption, as outlined in References 3,4, and 10. Once the initial plane of data has been generated, the marching procedure can then be applied over the remainder of the projectile.

The outer boundary, which consists of the bow shock emanating from the sharp nosetip of the projectile, is numerically fit using the implicit boundary procedure of Reference 10.

At the body surface, the pressure p_s is defined from $\frac{\partial p}{\partial \zeta} = 0$ across the subsonic sublayer, and a no slip boundary condition is imposed. For the case of a projectile possessing a finite spin rate ω , the velocities at the surface become:

$$u_w = 0 \quad v_w = r\omega \cos \phi \quad w_w = -r\omega \sin \phi \quad (2)$$

where ϕ is the roll angle measured from the windward side, using the sign convention as shown in Figure 3.

3. QUASI-STEADY APPROXIMATION

The governing equations for the PNS technique are derived on the basis of several assumptions about the flow field (e.g. supersonic, thin-layer approximation, et al). Of particular importance here is the fact that the flow fields of References 3 thru 7 share one characteristic which further ensures the suitability of the PNS approach; that is, they are steady flows.

For the present case of flow over a spinning non-axisymmetric projectile using a fixed coordinate system, the steady nature of the flow is lost. Even at $\alpha = 0^\circ$, a constant change in roll orientation of the projectile contributes a periodic unsteadiness to the flow field. In effect, this is an unsteady problem being modeled using a steady approach. Particular attention must be focused on the unsteady nature of this flow and the ramifications of its modeling using a steady approach.

To apply the PNS technique to the case of a spinning non-axisymmetric body is to assume that the flow is quasi-steady. Such an assumption implies that for some instant of time, the rates of change of the properties at every point in the computational domain are nearly zero. This is a reasonable assumption if the nondimensional spin rate, PD/V , is small enough.

A series of computations were run to determine a range of nondimensional spin rates over which the quasi-steady assumption was valid. Cases were run varying PD/V from small values to typical flight values. As shown in Figure 5, the computed roll damping was relatively insensitive to spin rate for the range $.005 < PD/V < .05$. The linear behavior of rolling moment with respect to spin rate allows the computed roll damping coefficient to be applied to the much higher spin rates that are typical of launch and flight conditions for shell.

IV. PRELIMINARY ANALYSIS

1. BACKGROUND

The current objective in the design of a training round with a non-conical boattail is to reduce its firing range. The larger de-spin moment acquired with a non-conical boattail is expected to induce gyroscopic instability faster than would a completely axisymmetric configuration. Gyroscopic instability is associated with a fast-growing average amplitude of angle of yaw.

For a symmetric body of revolution, the total drag behaves as a linear function of the square of the angle of yaw.¹¹ The general effect of the non-conical boattail on the spinning shell should therefore be increased drag due to the larger angles of attack experienced during flight. It is of primary interest in this study to determine the characteristics of such a configuration at small angle of attack.

Some aerodynamic effects of shell with non-axisymmetric boattails have previously been examined and give useful information in terms of what kind of performance to expect from a triangular non-conical boattail. Platou¹²⁻¹³ examined an array of projectiles with non-axisymmetric boattails in order to determine the merits of such shapes. Wind tunnel tests and range firings of configurations with non-conical boattails consistently indicated improved static stability over configurations with conical boattails.

The flat faces of the straight non-conical boattails were described in Reference 12 as "fin-like surfaces" possessing no differential cant. As such, boattails similar to the design of interest in this study were shown to have much higher roll damping than their axisymmetric counterparts. A two-caliber, 7° triangular boattail on a 5 to 7 caliber shell was shown through free-flight

testing at transonic speeds to have a roll damping coefficient an order of magnitude larger than a cylindrical boattail.*

Reference 12 also showed a significant dependence of the rolling moment on roll orientation and angle of attack. For the same configuration just mentioned $C_{l\alpha}$ was found to be of the same order of magnitude as C_{lp} .

More recently, wind tunnel roll-oscillation tests¹⁴ were performed on a shape quite similar to the one of interest in this study. The primary objective of the tests was to determine the dynamic stability characteristics in roll. The total length of the configuration was 6 calibers and the length of the 7° triangular non-conical boattail was 1 caliber. The large degree of uncertainty present in the reduced data (typically 50% of the total magnitude) makes the roll characteristics difficult to interpret qualitatively. At Mach 2, the roll damping was practically independent of boattail roll orientation; likewise, variation of roll damping did not occur as a function of angle of attack for $\alpha < 10^\circ$. The pitch-plane aerodynamics also showed little or no dependence on roll orientation, and in this sense the model was viewed as being nearly axisymmetric.

2. STATIC AERODYNAMIC ANALYSIS

Sign conventions for all aerodynamic coefficients discussed here are based on the coordinate system of Reference 11, shown in Figure 4.

According to Murphy¹¹, the rolling moment coefficient for a non-axisymmetric configuration can be written as:

$$C_l = \delta_f C_{l\delta} + (PD/V) C_{lp} + \delta C_{l\alpha} \quad (3)$$

It can be seen from Figure 2 that the triangular non-conical boattail is analogous to a set of three control surfaces with no differential cant; therefore $C_{l\delta}$ is zero. It remains then to determine the values of C_{lp} and $C_{l\alpha}$ for

the flight conditions of interest. If the yaw angle is zero, then the rolling moment coefficient can be described using the roll damping, C_{lp} , alone.

Similarly, if the projectile is not spinning, then the rolling moment coefficient can be described using $C_{l\alpha}$ alone. If the projectile is spinning at

some yaw angle, both remaining terms on the right-hand side of Equation (3) must be considered in evaluating the rolling moment.

* It is of interest to note that a major design objective in References 12 and 13 was to increase the range and accuracy of shell by employing a non-conical boattail. In order to maintain the gyroscopic stability of that family of shell, the next design change was to cant or twist the boattail to correspond to the gun barrel twist.

The simplest assumed form of C_{l_α} for an n-finned missile that satisfies the Maple-Synge¹⁵ requirement of analytic continuity in both pitch and roll is

$$C_{l_\alpha} = A \sin n\theta \quad (4)$$

where $A = k\delta^{n-1}$, $k = \text{constant}$.

For an axisymmetric body of revolution, $C_{l_\alpha} = 0$. For the projectile of interest in this study, $n = 3$; therefore the rolling moment contribution due to non-axisymmetry alone is periodic in 120° roll intervals. From Figure 2 and Equation (4), it is apparent that C_{l_α} is known for all roll orientations if it is known for $0^\circ < \theta < 60^\circ$.

More importantly, if such an assumed form for C_{l_α} is valid, then at a constant spin rate C_{l_α} must oscillate about zero at a frequency which is proportional to the spin rate. (We note that the PNS computation is carried out with a zero coning rate, therefore $P = \delta$.) If the spin rate is large enough, then the roll frequency becomes large compared to the pitch and yaw frequencies, and the integrated effect of C_{l_α} along the trajectory becomes nil.

The spin rates of spin-stabilized shells are normally quite large compared to those of fin-stabilized projectiles. The determination of a minimum spin rate at which the effect of C_{l_α} can no longer be ignored in the prediction of projectile flight is unclear; the judgement concerning the importance of the effect at various spin rates is not addressed here. It is, however, desirable to establish the relative magnitudes of such oscillations compared to the nominal values of the computed aerodynamic coefficients. Section V will discuss further the effect of roll orientation on the static aerodynamic coefficients.

The PNS code is employed to compute the flow field over the shell by spatially marching the solution downstream. In general, the solution is no longer valid when regions of axial separation or subsonic flow are encountered. Therefore, the domain of the PNS computation does not include the base region. The rolling and pitch-plane aerodynamic characteristics of shells are not overly sensitive to base effects in the supersonic flight regime. The same cannot be said about axial force since base drag at the Mach numbers of interest is a significant component of the total drag.

For these reasons a second computer code - MC DRAG¹⁶ - is used to aid in the analysis of drag for the shell of interest. MC DRAG is a fast running, easy to use program which employs empirical data, low order approximations, and similarity concepts to estimate the components of zero-yaw drag as functions of Mach number. For this study, it is of main interest to apply MC DRAG to obtain estimates of base drag for the non-axisymmetric shapes.

Following the notation of Reference 16, the zero-yaw drag coefficient takes the form:

$$C_{D_0} = C_{D_H} + C_{D_{BT}} + C_{D_B} + C_{D_{SF}} \quad (5)$$

Furthermore, the total forebody drag coefficient is defined as:

$$C_{D_F} = C_{D_H} + C_{D_{BT}} + C_{D_{SF}} \quad (6)$$

In order to obtain base drag estimates for the non-axisymmetric shapes from MC DRAG, a simple geometric model for the non-conical boattail must be established. This is necessary because MC DRAG can only be applied to boattails which are conical.

Figure 6 shows the cross-sectional areas as functions of axial position for two of the boattails under consideration. Each configuration consists of the same nose and cylindrical midsection, differing only in the boattail geometry. One is a 7° conical boattail and the other is the triangular non-conical boattail described in Section II.

It is well known that base drag is a strong function of the cross-sectional area of the base. For a given length, C_{D_B} for the non-conical boattail should be bounded by C_{D_B} for the 7° conical boattail and the cylindrical extension. Thus, the base drag for the non-axisymmetric configuration has been estimated from the drag of a conical boattail which possesses an equivalent base area.** No further distinction is made between the non-axisymmetric shape and this simple geometric model in the ensuing discussion of drag.

V. RESULTS

Solutions were generated over both conical and non-conical boattails using an algebraic grid. The grid consisted of 45 exponentially-stretched points in the radial direction from the body to the shock and spacing of points circumferentially around the body at 5° intervals. Grid spacing at the wall was maintained such that the first point above the body was contained in the laminar sublayer (specifically, a value of $3 < y^+ < 5$ was used to maintain adequate viscous resolution).

** Reference 1 examined an "equivalent area" boattail shape to model the non-conical boattail, unlike the geometric model employed here. The equivalent area boattail was an axisymmetric configuration whose cross-sectional area was equal to that of the non-conical boattail at all axial locations.

All numerical computations were performed on a CDC 7600 computer with a speed of .0026 CPU sec/step/grid point (number of grid points/step = 45 x 72). The computer time required to obtain a starting solution and march to an axial position just upstream of the boattail was typically 2000 CPU seconds. Another 1000 CPU seconds were required to march over each of the 3 different boattail configurations.

1. ROLL DAMPING

Figure 7 shows the roll damping coefficient, C_{ℓ_p} , developing over the shell of interest at Mach 5. Comparison is made between the non-conical boattail configuration and the two axisymmetric configurations. It is apparent that the full 2 caliber non-conical boattail generates an order of magnitude increase in roll damping compared to the axisymmetric configurations. The order of magnitude increase in roll damping for the non-conical configuration is almost entirely attributable to surface pressure rather than viscous effects.

Figure 8 shows the development of C_{ℓ_p} over the non-axisymmetric shell for Mach numbers 1.5, 3 and 5. It is apparent that the effect of C_{ℓ_p} decreases with increasing Mach number in this speed regime. Slight oscillations in the predicted roll damping occur for the non-axisymmetric body. These oscillations are a result of grid coarseness in the circumferential direction, which affects the solution near the parabolic intersections of the boattail cone and beveled flats. Figure 9 presents the roll damping as a function of Mach number using boattail length as a parameter.

Figure 10 compares the computed C_{ℓ_p} to that obtained from range firings¹⁷ for the 1/2 caliber non-conical boattail configuration. Range reductions showed that not all experimental data points were well-determined, therefore some scatter exists. Disagreement between computation and experiment below Mach 3 is from 0% to 20%, while disagreement near Mach 5 is about 30%.

2. PITCH-PLANE AERODYNAMICS

Figure 11 shows the development of normal force coefficient over the shell for conical and non-conical boattails at Mach 1.5. Only slight differences exist in the normal force due to the three different boattails. Figure 12 shows the small- α slope of the normal force coefficient for the non-conical configuration as a function of Mach number using boattail length as a parameter. Figure 13 uses the same approach to present the pitch-plane center of pressure. Both C_{N_α} and CP are seen to be non-linear with respect to boattail length.

Pitching moment coefficients are presented here with reference to the centers of gravity of each individual configuration. Table 1 shows the c.g.'s for the various configurations, assuming solid, isotropic material. The only addition is a .5 caliber non-conical boattail case, possessing a small base cavity, and used in the firing range comparison.

Figure 14 shows the small- α slope of the pitching moment coefficient for the non-axisymmetric configuration as a function of Mach number, using boattail length as a parameter. It is apparent that $C_{m\alpha}$ decreases with increasing Mach number, and increases somewhat linearly with increasing boattail length.

Figure 15 compares the computed $C_{m\alpha}$ to that obtained from range firings for the 1/2 caliber non-conical boattail configuration with small base cavity. Disagreement between computation and experiment is at most 5%.

Figures 16, 17, 18 and 19 compare values of pitching moment coefficient for configurations having conical and non-conical boattails, keeping boattail length fixed. For a boattail of length 1/2 caliber, differences in pitching moment due to boattail shape can barely be discerned. As boattail length increases, these differences become more apparent. In general, the fin-like influence of the non-conical boattail is demonstrated by the more stable values of pitching moment compared to the axisymmetric shapes.

3. DRAG

Figures 20 and 21 show the total forebody drag developing over the axisymmetric and non-axisymmetric shell for Mach numbers 1.5 and 3, respectively. Comparison is made with the predicted values from MC DRAG. For each case, C_{D_F} for the non-axisymmetric shape falls between C_{D_F} for the two axisymmetric shapes. Figure 22 shows C_{D_F} from the PNS code for the non-axisymmetric shape as a function of Mach number using boattail length as a parameter. Figure 23 shows the base drag for the non-axisymmetric shape obtained from MC DRAG as a function of Mach number, using boattail length as a parameter.

Figure 24 shows the predicted total drag of the non-axisymmetric shell as a function of Mach number, using boattail length as a parameter. The total drag is obtained by combining the forebody drag from PNS and the base drag from MC DRAG. It is apparent that the total drag decreases with increasing Mach number and decreases slightly with increasing boattail length.

Figure 25 compares the predicted total drag with that obtained from range firings. Disagreement below Mach 3 is within 10%, while disagreement near Mach 5 is about 20%.

4. ROLL ORIENTATION

The effect of roll orientation on the roll and pitch-plane aerodynamic coefficients is summarized in Table 2. Cases were run for 5 roll orientations at 2° angle of attack and no spin. For non-conical boattail lengths of 1 and 2 calibers, the computations showed little effect of roll orientation on $C_{N\alpha}$, C_P , or $C_{m\alpha}$. The largest variation of $C_{m\alpha}$ was about 5%, occurring for the case of Mach 1.5 with a 2 caliber non-conical boattail.

Table 2 also shows the computed rolling moments for each case. Using these results and the form for $C_{l\alpha}$ already discussed in Section IV, the amplitude A of the sinusoidal rolling moment was obtained for each case and is shown. Note that the form for $C_{l\alpha}$ employed here takes roll orientation into account; therefore, the amplitude A of $C_{l\alpha}$ at a given Mach number, angle of attack, and boattail length should be equal for all roll orientations. From symmetry, the rolling moments for $\theta = 0^\circ$ and $\theta = 60^\circ$ should equal zero, and the maximum rolling moment should occur at $\theta = 30^\circ$. It is apparent that the values for $C_{l\alpha}$ and A in Table 2 do not satisfy Equation 5 adequately. Two possible reasons are (1) Equation (4) is an over-simplified form for $C_{l\alpha}$, or (2) numerical damping in the PNS solution inhibits precise determination of $C_{l\alpha}$ for a nearly axisymmetric body.

From the results presented thus far and the form for $C_{l\alpha}$ discussed in Section IV, it can be deduced that even at moderate angles of attack the rolling moment induced by $C_{l\alpha}$ on the flight of the projectile is negligible compared to that which is induced by C_{lp} . At Mach 1.5, with a 1 caliber non-conical boattail and a non-dimensional spin rate $PD/V = .1417$ (launch condition), the computed C_{lp} gives a rolling moment of approximately $C_{l\alpha} = -.0085$. At $\alpha = 10^\circ$ the computed $C_{l\alpha}$ (disregarding non-linear effects) gives a maximum rolling moment of approximately $C_{l\alpha} = -.00021$, at least an order of magnitude less than the contribution due to C_{lp} .

Similarly, the maximum side moment produced by geometric non-symmetry about the pitch-plane was compared to Magnus moment at each Mach number. Following the same form as Equation 5, the computed maximum geometric side moment occurred for $\theta = 30^\circ$. For the 1/2 caliber non-conical boattail configuration, the maximum geometric side moment was computed to be at least an order of magnitude less than the Magnus moment at launch spin rate.

It was concluded that roll orientation has a negligibly small effect on pitch plane, roll damping and Magnus coefficients for the cases where the NCBT is less than one caliber. Variations of these coefficients with respect to roll orientation were ignored in the trajectory simulations which are presented.

5. TRAJECTORY SIMULATION

In order to aid in the design of a range-limited projectile, the computed aerodynamic coefficients were applied to a mathematical simulation of the projectile in flight. A six degree-of-freedom computer code was used to integrate the equations of motion for a rigid projectile.¹⁸ Using as input

the aerodynamic forces and moments computed in this study, ranges at which the gun-launched non-axisymmetric configurations would experience large increases in yaw angle were determined.

The trajectory simulation code requires the physical properties of the projectile (see Table 1) and initial flight conditions. In addition, an array of aerodynamic coefficients must be specified as functions of Mach number and angle of attack. Some coefficients, such as pitch damping ($C_{m_q} + C_{m_{\dot{\alpha}}}$) and cubic pitching moment ($C_{m_{\alpha^3}}$), may have a significant effect on the trajectory, but are not directly available and must be estimated. The overall effect of such estimations was gauged through parametric variations with guidance from Reference 19.

The launch velocity is taken to be Mach 4.78.²⁰ The gun twist is taken to be 23.94 calibers/revolution²⁰ and the launch elevation is set at 35.55 mils (2°). The initial angle of attack is taken to be zero. The initial pitch rate is taken to be 10 radians/second, in order to provide a first maximum yaw between 1° and 2°.

Results from trajectory simulations are presented here for two configurations: 1/2 caliber and 3/4 caliber non-conical boattail shell. As previously mentioned, the total lengths of these two shells differ by 1/4 caliber.

Figure 26 shows Mach number as a function of range for the two configurations. Both shells maintained forward flight long enough to reach Mach 1, occurring at ranges between 2000 and 2500 meters. Figure 27, which shows total yaw angle vs. range, reveals very different behavior between the two shells. The 1/2 caliber non-conical boattail shell experienced small growth in yaw over the entire trajectory, whereas the 3/4 caliber non-conical boattail shell reached yaw angles of 8° by 1000 meters. It is clear from Figures 26 and 27 that the large yaw experienced by the longer shell caused significant loss in velocity due to the higher drag.

Figure 28 shows nondimensional spin rate PD/V vs. range. The 1/2 caliber boattail shell experienced a continual increase in PD/V out to 2500 meters. The 3/4 caliber boattail shell, due to higher roll damping, maintained a relatively constant PD/V.

Figure 29 shows gyroscopic stability¹¹ vs. range. At launch, both shells possess $S_g < 1.5$, which is a nominal value for spin-stabilized projectiles. The 1/2 caliber boattail shell experienced a continual increase in S_g out to 2500 meters. The 3/4 caliber boattail shell experienced a decrease in S_g , falling below 1.0 at a range of about 600 meters, and climbing above 1.0 through the remainder of the trajectory.

VI. CONCLUSIONS

A computational aerodynamics study has been made for an initial design configuration intended as a sub-caliber training round for a 25mm gun. The configuration has a triangular non-conical boattail which induces a large de-spin moment. The thin-layer Parabolized Navier-Stokes computational technique was used to compute the static aerodynamic coefficients acting on the shell at supersonic speeds.

The computations showed that a full 2 caliber, 7°, triangular non-conical boattail increases the roll damping by more than an order of magnitude compared to axisymmetric configurations of the same caliber and length. The computed roll damping for the case of a 1/2 caliber non-conical boattail is almost double that of an axisymmetric configuration of the same caliber and length.

The pitch plane results verified that the non-conical boattail gives the shell a more statically stable behavior compared to axisymmetric configurations. The computed drag of the non-axisymmetric shell was consistently bounded by the drag of a shell with a 0° boattail and a shell with a conical boattail with the same slope as the beveled cuts as the non-conical boattail. The effect of roll orientation on the pitch-plane, Magnus, and rolling forces and moments was found to be negligible for small angles of attack.

Comparison of computed aerodynamic coefficients to recently obtained firing range data yielded the following: (1) roll damping coefficient agreed from 0% to 20%, except near Mach 5, where agreement was within 30%; (2) linear pitching moment coefficient agreed within 5%; and (3) zero yaw drag coefficient agreed within 10%, except near Mach 5, where agreement was within 20%.

Six degree-of-freedom trajectory simulations, based on computationally determined static aerodynamic coefficients, were computed for 1/2 and 3/4 caliber non-conical boattail configurations. The 1/2 caliber non-conical boattail shell maintained small angles of yaw past 2500 meters in range. The 3/4 caliber boattail shell reached moderate angles of yaw within a range of 1000 meters. Since computed aerodynamic coefficients were not available below Mach 1, no assessment was made of the flight performance of the shell beyond a range of 2500 meters.

TABLE 1. Physical Characteristics of Configurations of Interest; Material: Steel.

TOTAL LENGTH	BOATTAIL LENGTH	BOATTAIL CONFIGURATION	C.G. (cal from nose)	Mass (g)	MOMENTS OF INERTIA (g-cm ²)	
					AXIAL I _x	TRANSVERSE I _y
3.75	0	none	2.60	30.7	5.53	37.0
4.00	0.25	7° non-conical	2.74	34.5	6.37	47.4
4.25	0.5	0°	2.88	38.3	7.25	59.9
		7° conical	2.85	37.4	6.88	48.5
		7° non-conical	2.87	38.1	7.16	59.2
		7° non-conical w/base cavity	2.78	----	----	----
4.50	0.75	7° non-conical	2.99	41.5	7.86	72.4
4.75	1.0	0°	3.14	45.9	8.98	91.4
		7° conical	3.04	42.5	7.65	64.0
		7° non-conical	3.11	44.6	8.47	86.8
5.25	1.5	0°	3.41	53.5	10.71	133.4
		7° conical	3.20	46.1	8.06	82.0
		7° non-conical	3.31	49.9	9.41	118.5
5.75	2.0	0°	3.67	61.0	12.43	187.5
		7° conical	3.31	48.6	8.24	100.2
		7° non-conical	3.47	53.9	9.97	151.0

TABLE 2. Effect of Roll Orientation on Various Static Aerodynamic Coefficients.

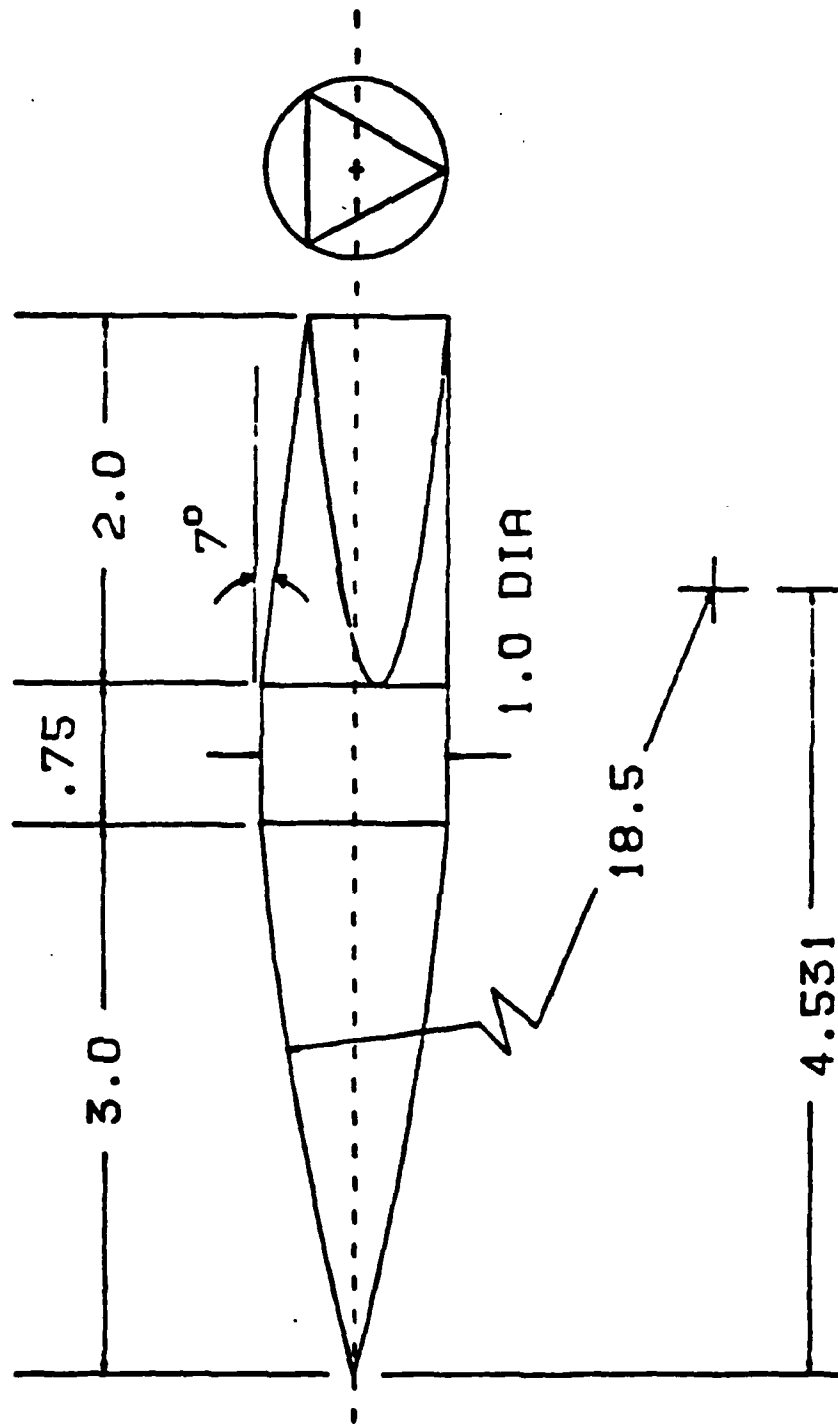
A. 1 Caliber Non-Conical Boattail Case, $\delta = 2^\circ$, PD/V = 0

	<u>Roll Orientation θ</u>					
	<u>0°</u>	<u>15°</u>	<u>30°</u>	<u>45°</u>	<u>60°</u>	<u>% var</u>
Mach No. = 1.5						
C_{N_α}	2.75	2.76	2.78	2.81	2.82	2.5%
CP	2.21	2.21	2.23	2.25	2.26	2.2%
C_{m_α}	2.46	2.46	2.43	2.40	2.38	3.3%
C_L	3.8×10^{-9}	-2.7×10^{-5}	-4.3×10^{-5}	-1.7×10^{-5}	3.6×10^{-9}	---
A	----	-.0011	-.0012	-.00069	----	---
Mach No. = 3						
C_{N_α}	2.86	2.86	2.86	2.86	2.86	0.0%
CP	2.37	2.37	2.37	2.37	2.37	0.0%
C_{m_α}	2.10	2.10	2.10	2.10	2.10	0.0%
C_L	3.0×10^{-11}	1.1×10^{-5}	1.5×10^{-5}	9.5×10^{-6}	6.1×10^{-11}	---
A	----	.00045	.00043	.00038	----	---
Mach No. = 5						
C_{N_α}	2.59	2.59	2.59	2.59	2.58	0.0%
CP	2.30	2.30	2.30	2.30	2.30	0.0%
C_{m_α}	2.09	2.09	2.09	2.09	2.08	0.0%
C_L	2.4×10^{-11}	7.3×10^{-6}	1.1×10^{-5}	6.7×10^{-6}	3.4×10^{-11}	---
A	----	.00030	.00032	.00056	----	---

TABLE 2. Effect of roll Orientation on Various Static Aerodynamic Coefficients. (Continued)

B. 2 Caliber Non-Conical Boattail Case, $\delta = 2^\circ$, PD/V = 0

	<u>Roll Orientation θ</u>					
	<u>0°</u>	<u>15°</u>	<u>30°</u>	<u>45°</u>	<u>60°</u>	<u>% Var</u>
Mach No. = 1.5						
C_{N_α}	2.64	2.67	2.71	2.77	2.80	5.9%
CP	2.09	2.12	2.16	2.21	2.24	6.9%
C_{m_α}	3.58	3.53	3.47	3.41	3.36	6.3%
C_L	3.9×10^{-9}	-4.1×10^{-5}	-9.9×10^{-5}	-7.2×10^{-5}	3.8×10^{-9}	---
A	----	-.0017	-.0028	-.0029	----	---
Mach No. = 3						
C_{N_α}	3.04	3.05	3.08	3.11	3.12	2.6%
CP	2.55	2.56	2.58	2.60	2.61	2.3%
C_{m_α}	2.71	2.69	2.65	2.61	2.59	4.7%
C_L	2.2×10^{-10}	2.7×10^{-6}	1.3×10^{-5}	1.4×10^{-5}	4.9×10^{-11}	---
A	----	.00011	.00052	.00056	----	---
Mach No. = 5						
C_{N_α}	2.74	2.74	2.74	2.75	2.75	0.0%
CP	2.45	2.46	2.46	2.47	2.47	0.0%
C_{m_α}	2.70	2.69	2.69	2.67	2.67	1.1%
C_L	4.2×10^{-11}	1.4×10^{-5}	2.3×10^{-5}	1.9×10^{-5}	5.1×10^{-11}	---
A	----	.00057	.00066	.00077	----	---



DIMENSIONS IN CALIBERS (ONE CALIBER = 13.5 mm)

Figure 1. Non-axisymmetric shell configuration.

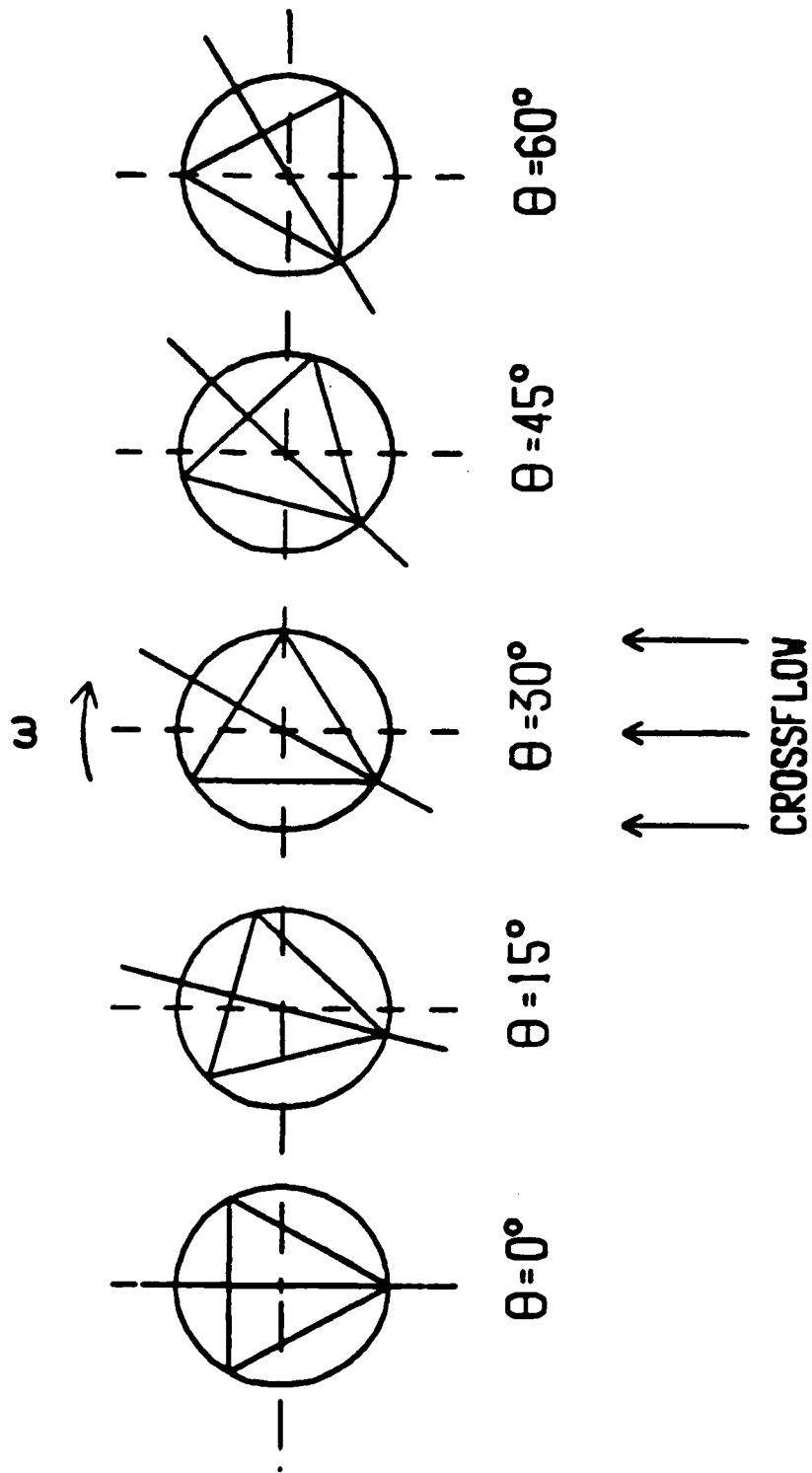


Figure 2. Roll orientation and direction of spin looking upstream.

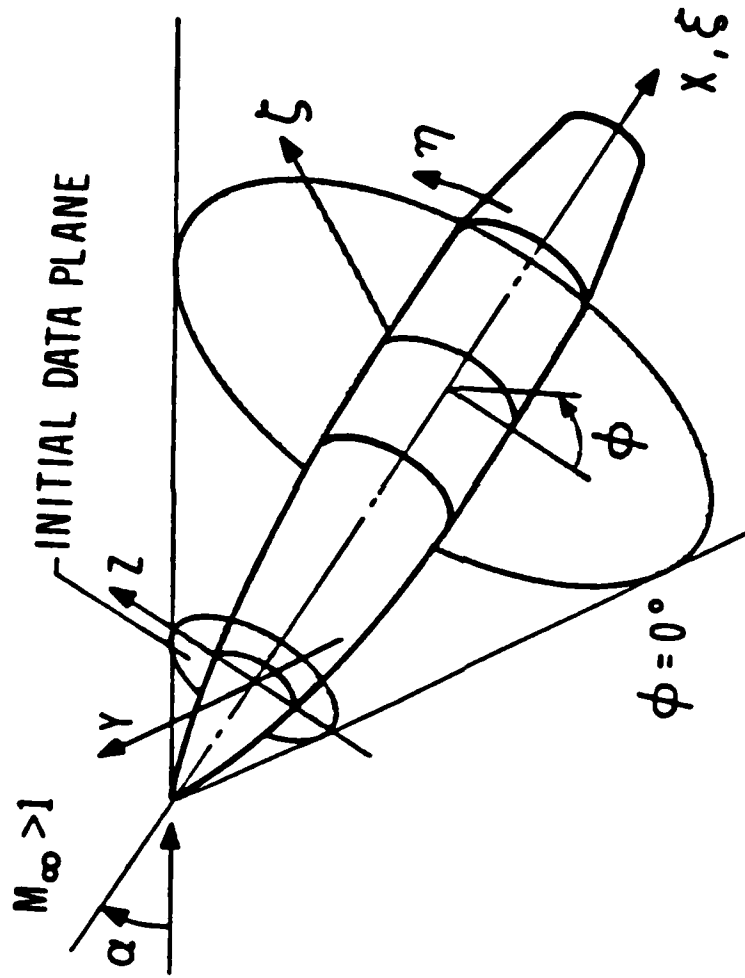


Figure 3. Physical and computational grid coordinates and notation.

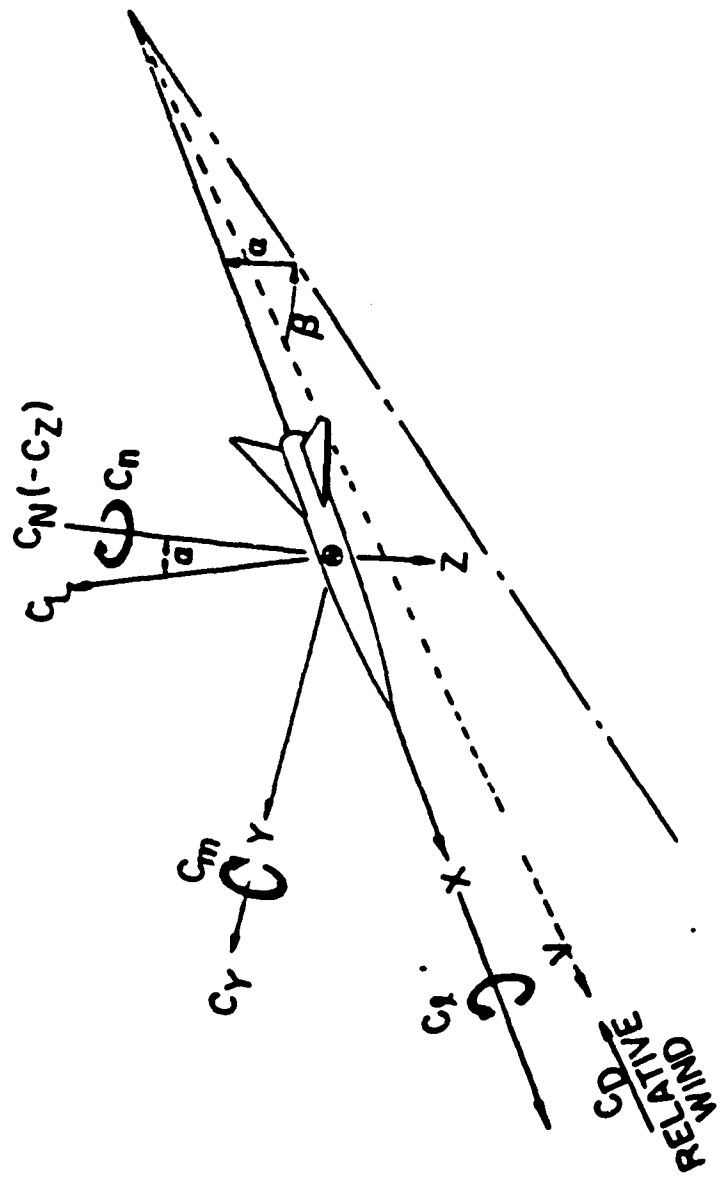


Figure 4. Coordinate system/sign conventions for aerodynamic coefficients.

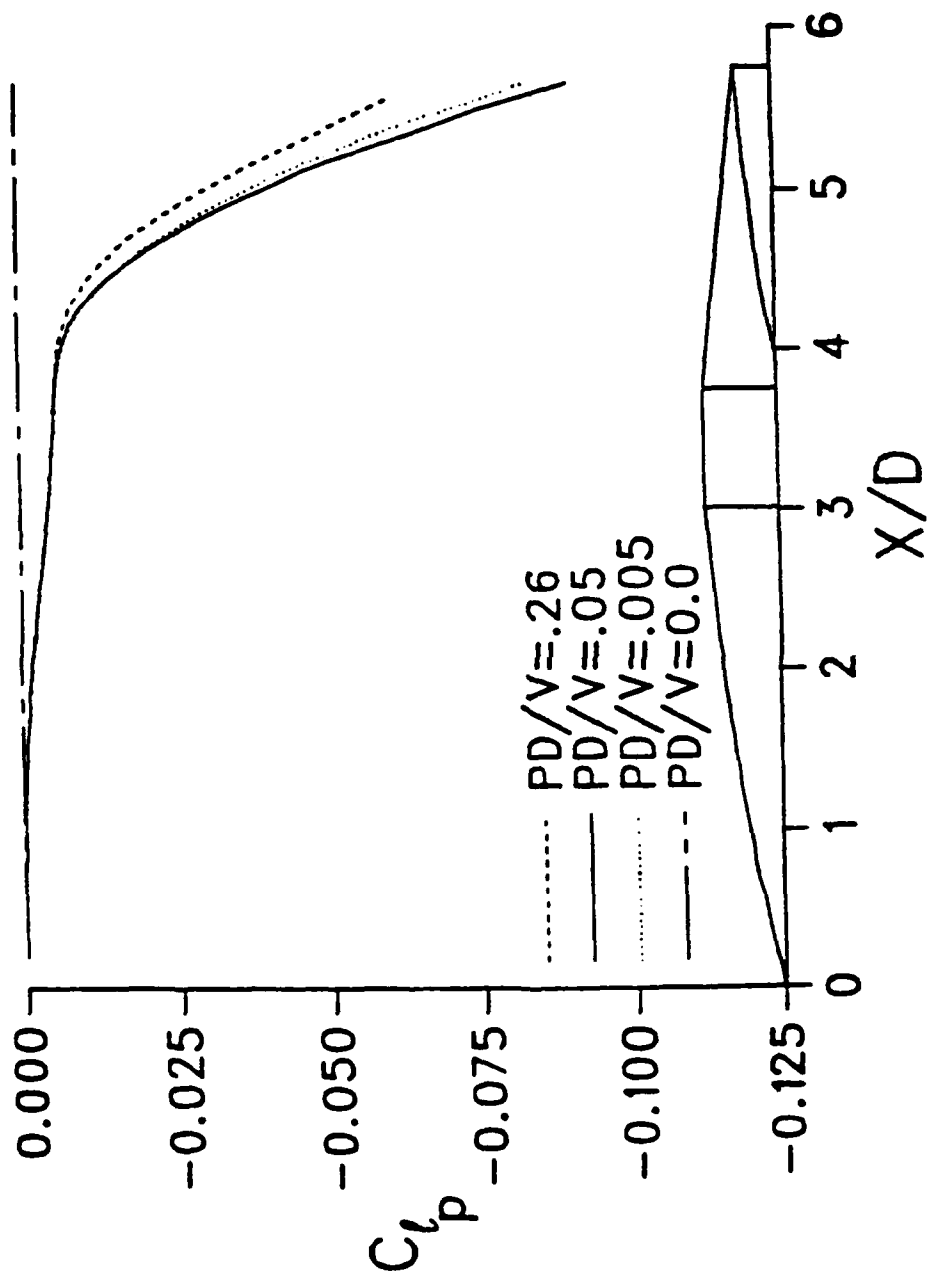


Figure 5. Validation of quasi-steady assumption for roll damping, Mach = 5, $\alpha = 0^\circ$, non-axisymmetric configuration.

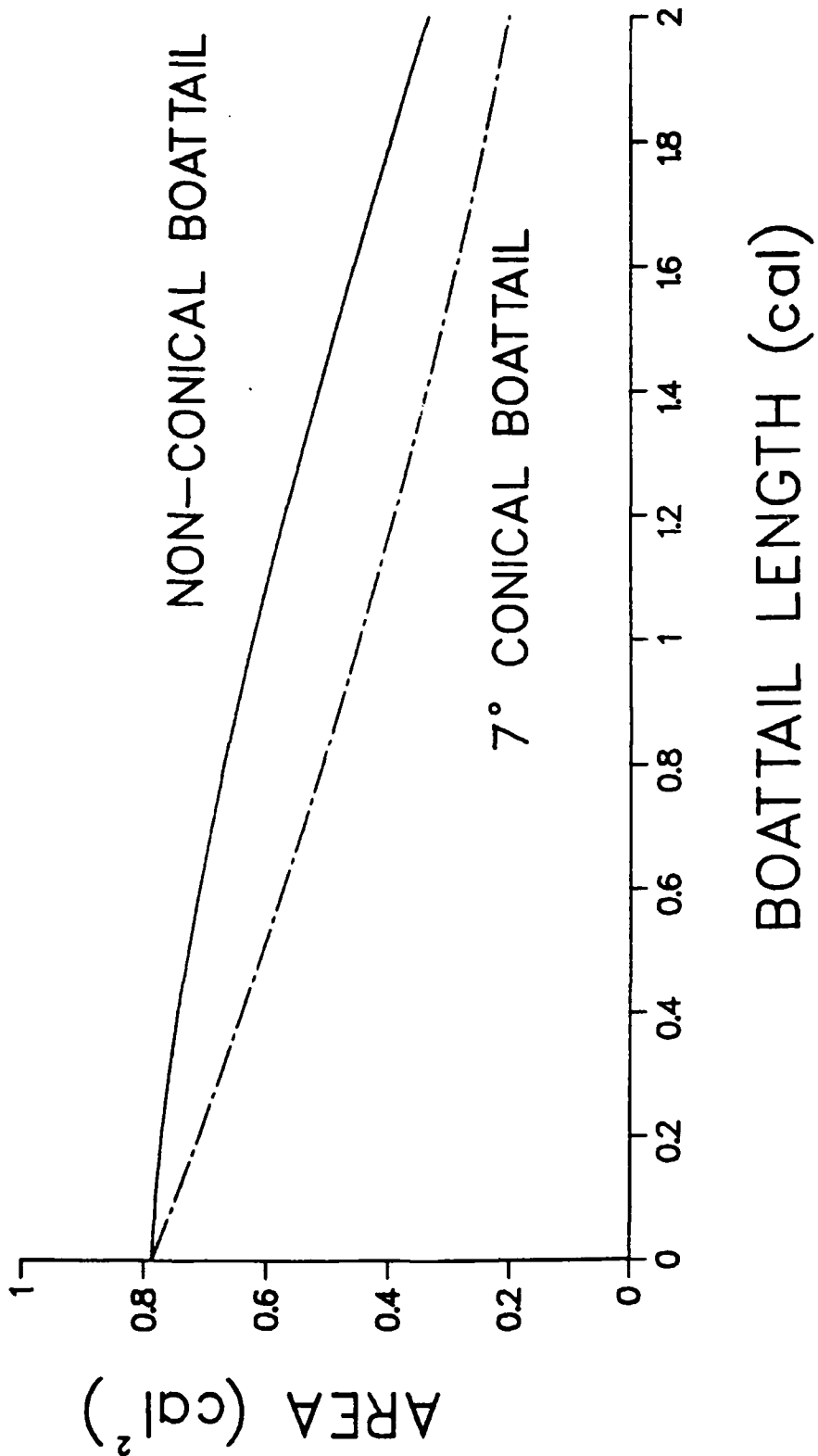


Figure 6. Cross-sectional areas of triangular non-conical boattail and 7° conical boattail as functions of axial position.

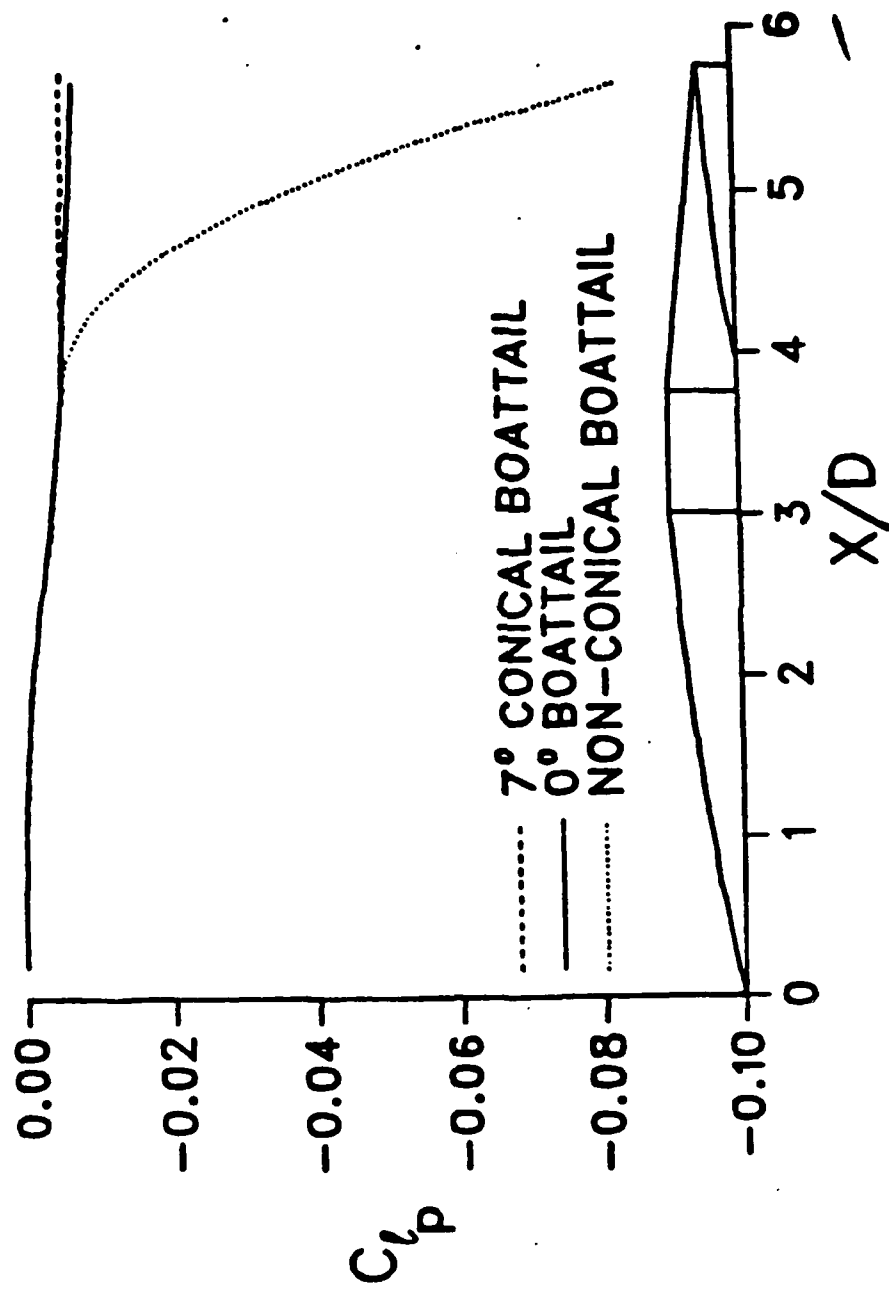


Figure 7. Roll damping developing over body, Mach = 5, $\alpha = 0^\circ$, axisymmetric and non-axisymmetric configurations.

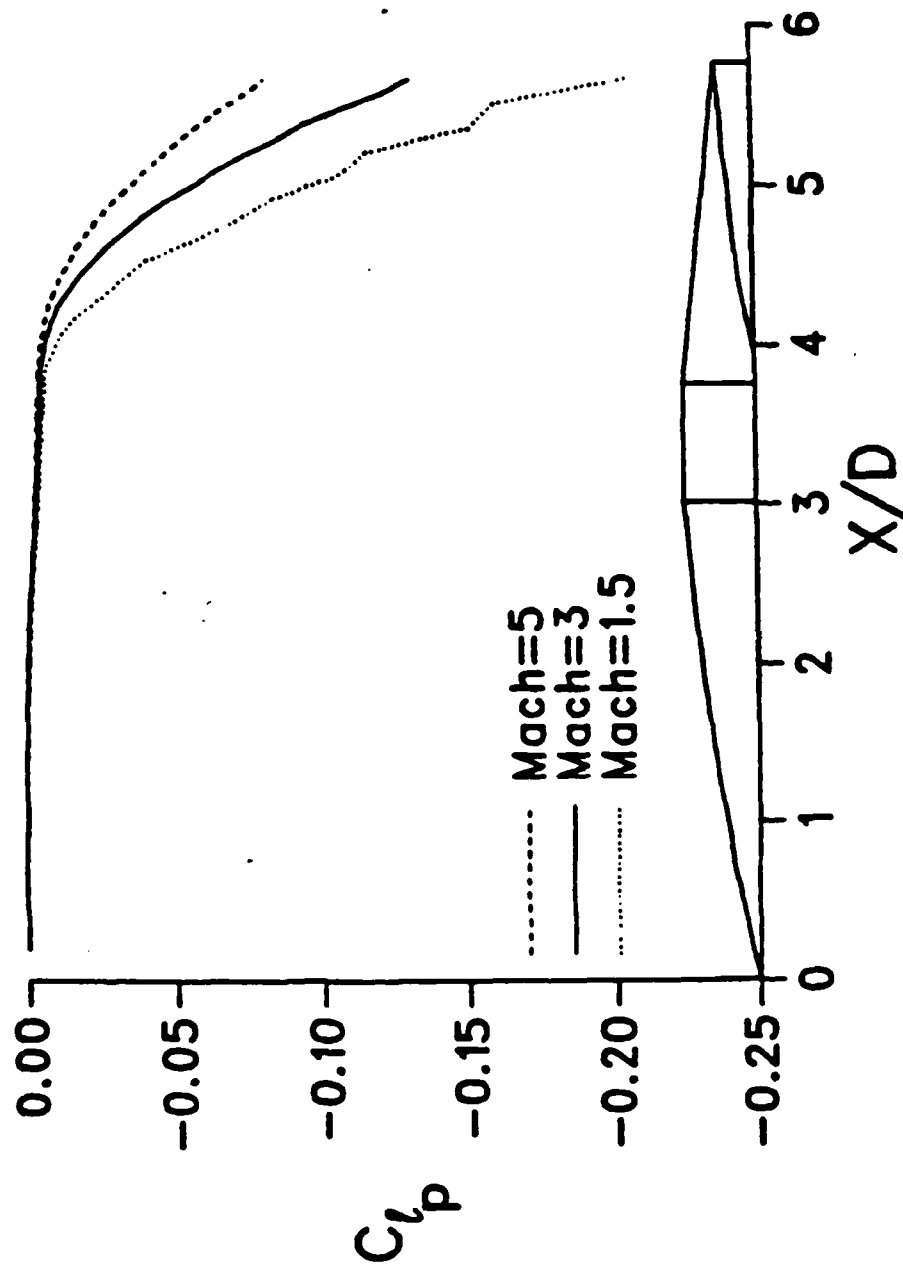


Figure 8. Roll damping developing over body, $\alpha = 0^\circ$, non-axisymmetric configuration.

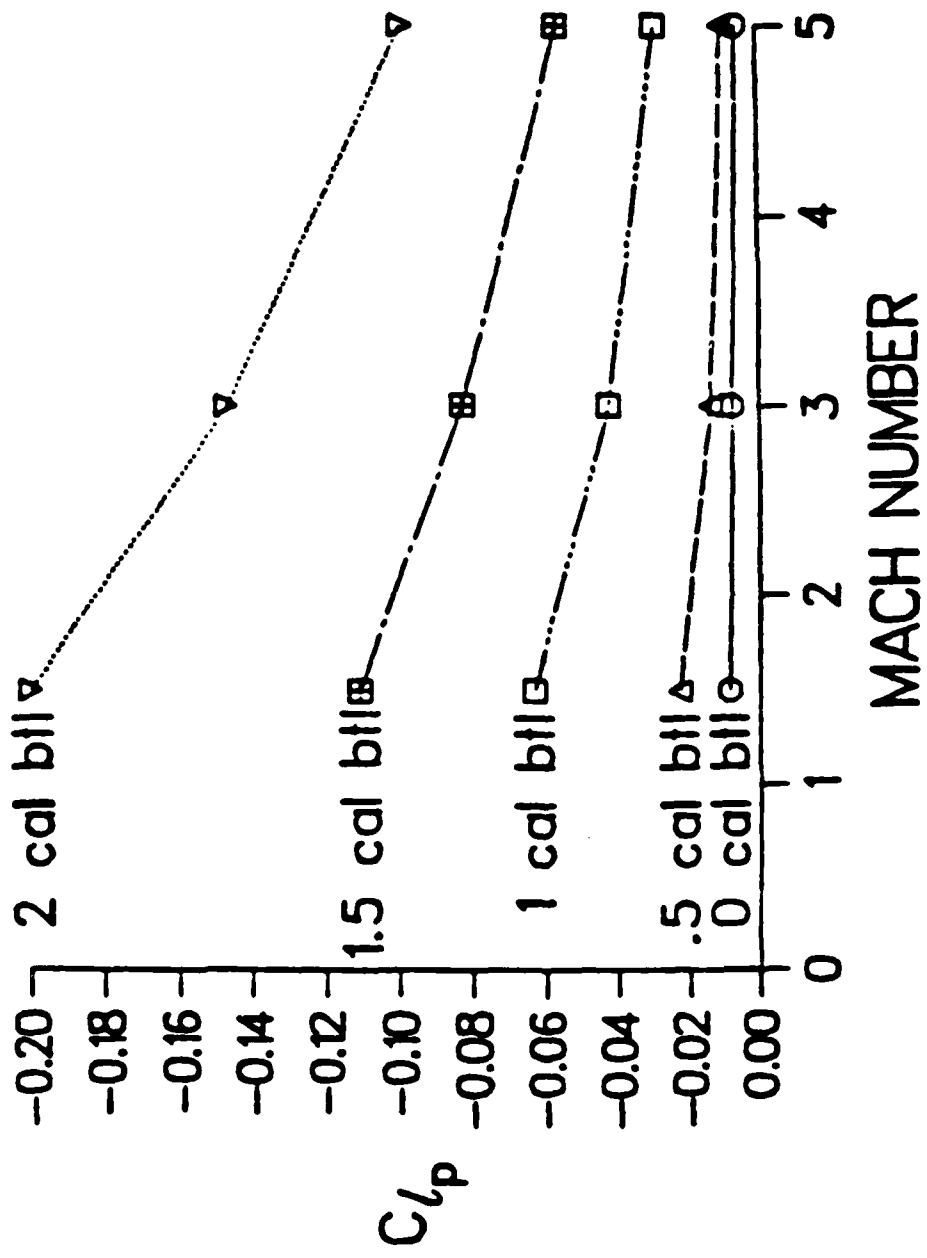


Figure 9. Roll damping of non-axisymmetric configuration with different boattail lengths, $\alpha = 0^\circ$.

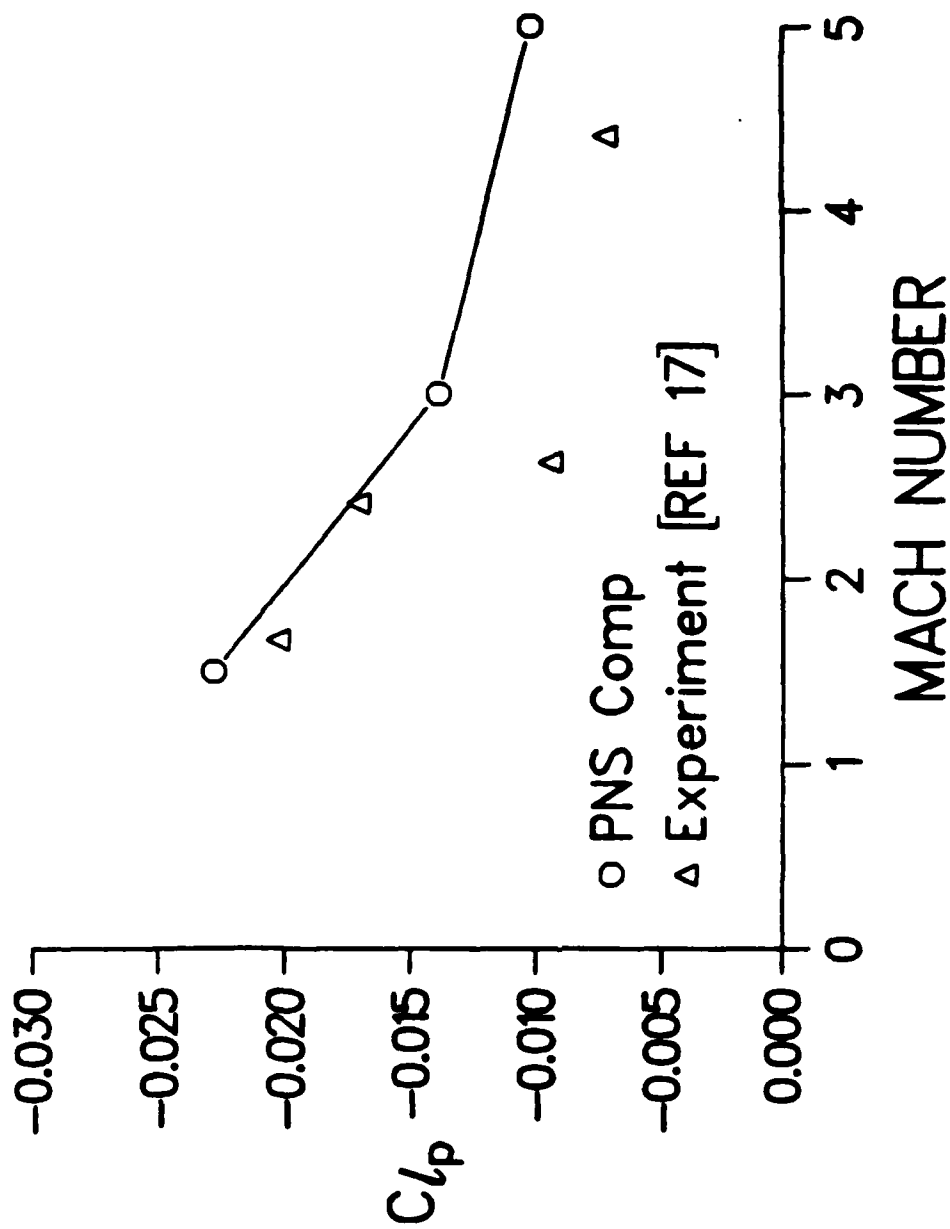


Figure 10. Roll damping of 1/2 caliber non-conical boattail configuration; comparison between computation and experiment.

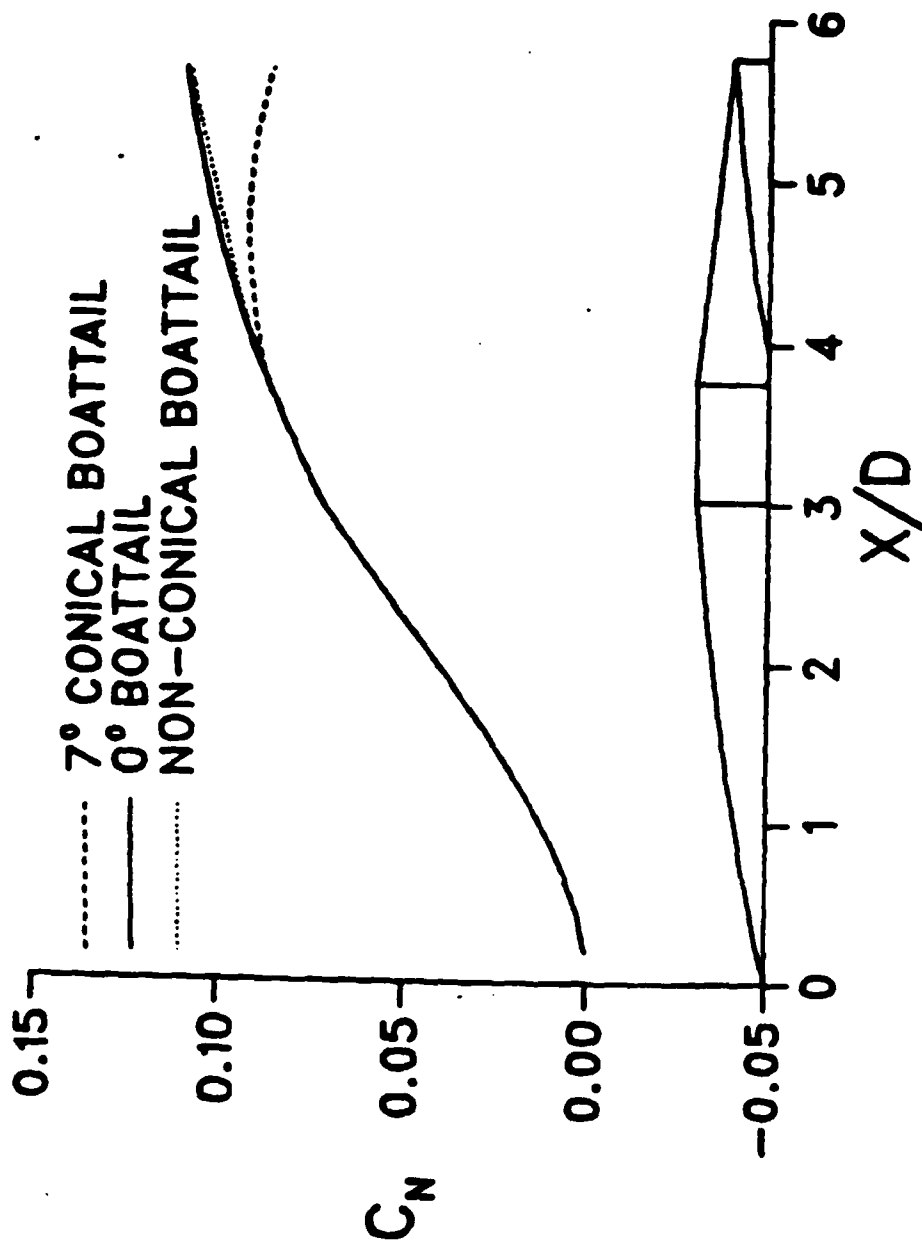


Figure 11. Normal force coefficient developing over body, Mach = 3, $\alpha = 2^\circ$, axisymmetric and non-axisymmetric configurations.

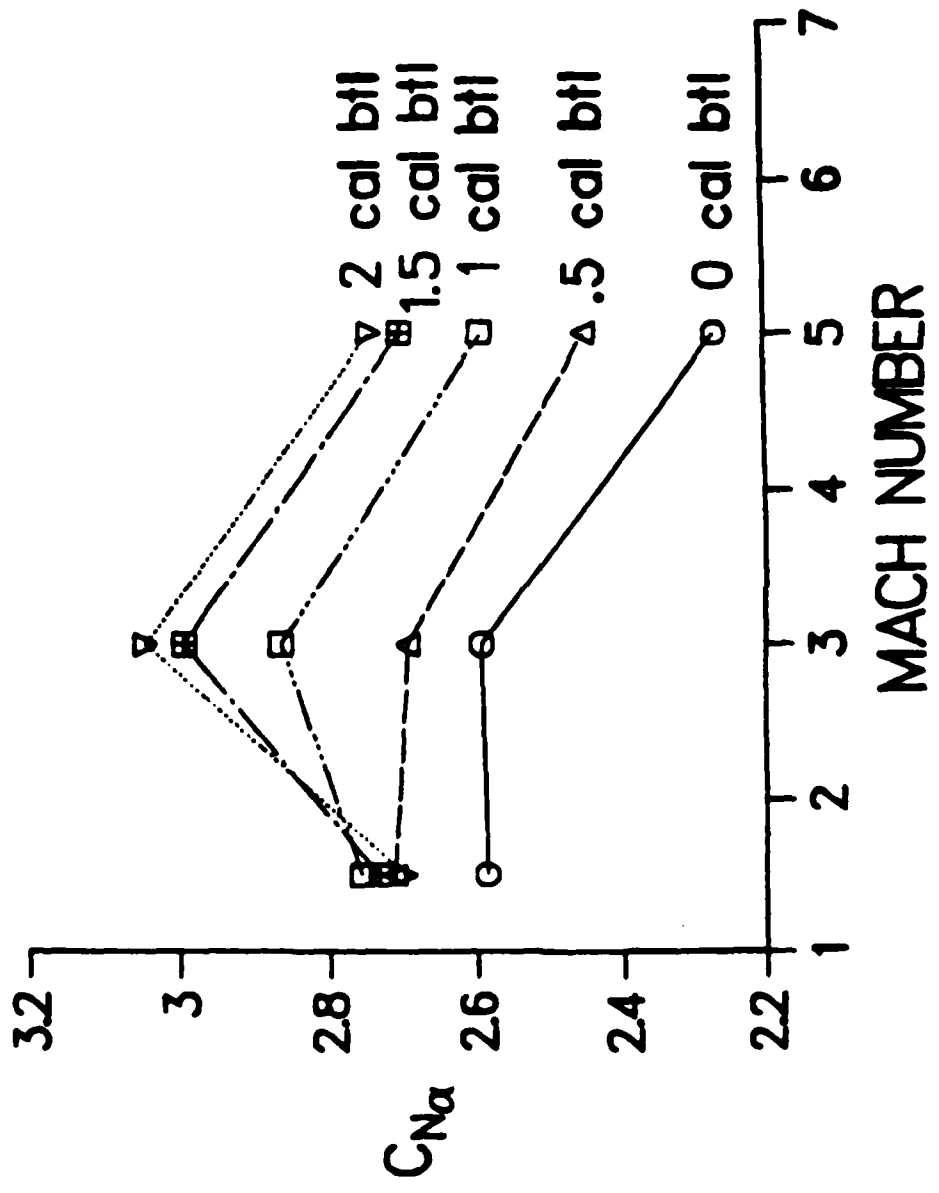


Figure 12. Slope of normal force coefficient for non-axisymmetric configuration with different boattail lengths.

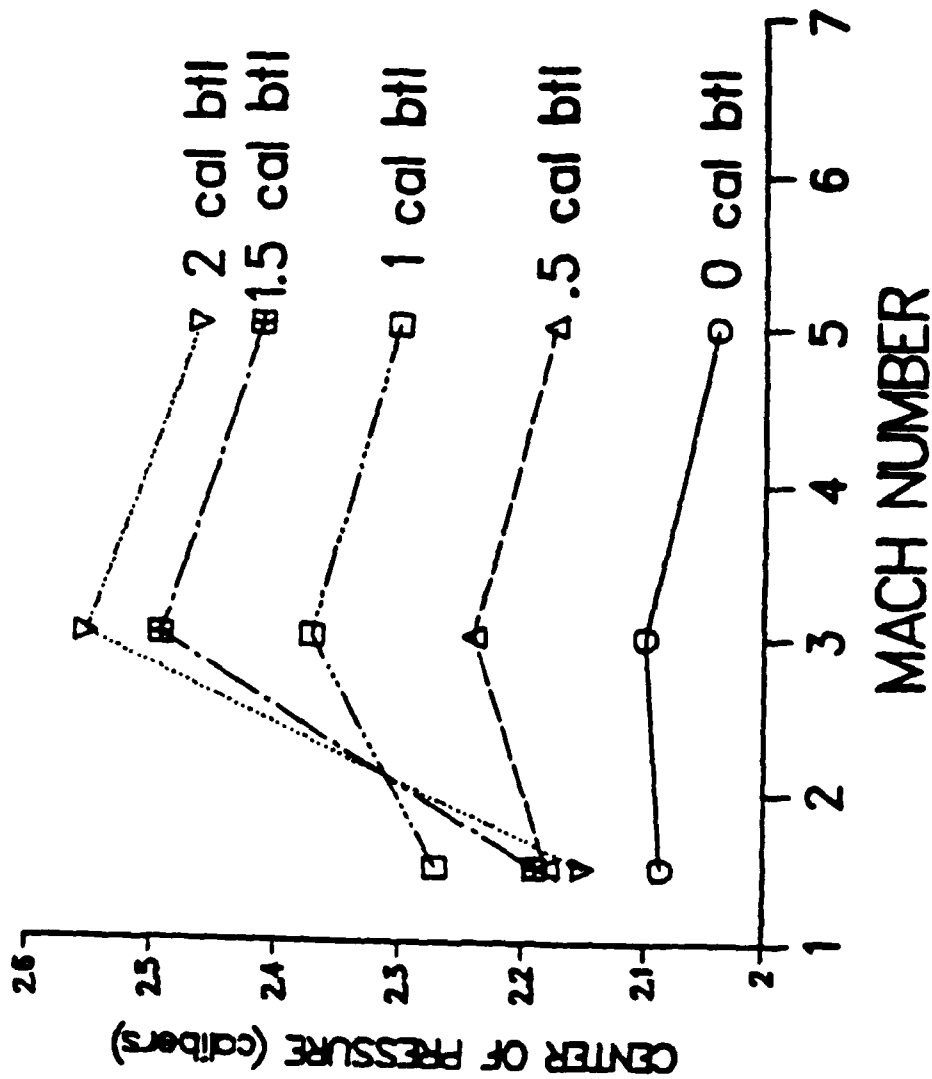


Figure 13. Pitch-plane center of pressure for non-axisymmetric configuration with different boattail lengths.

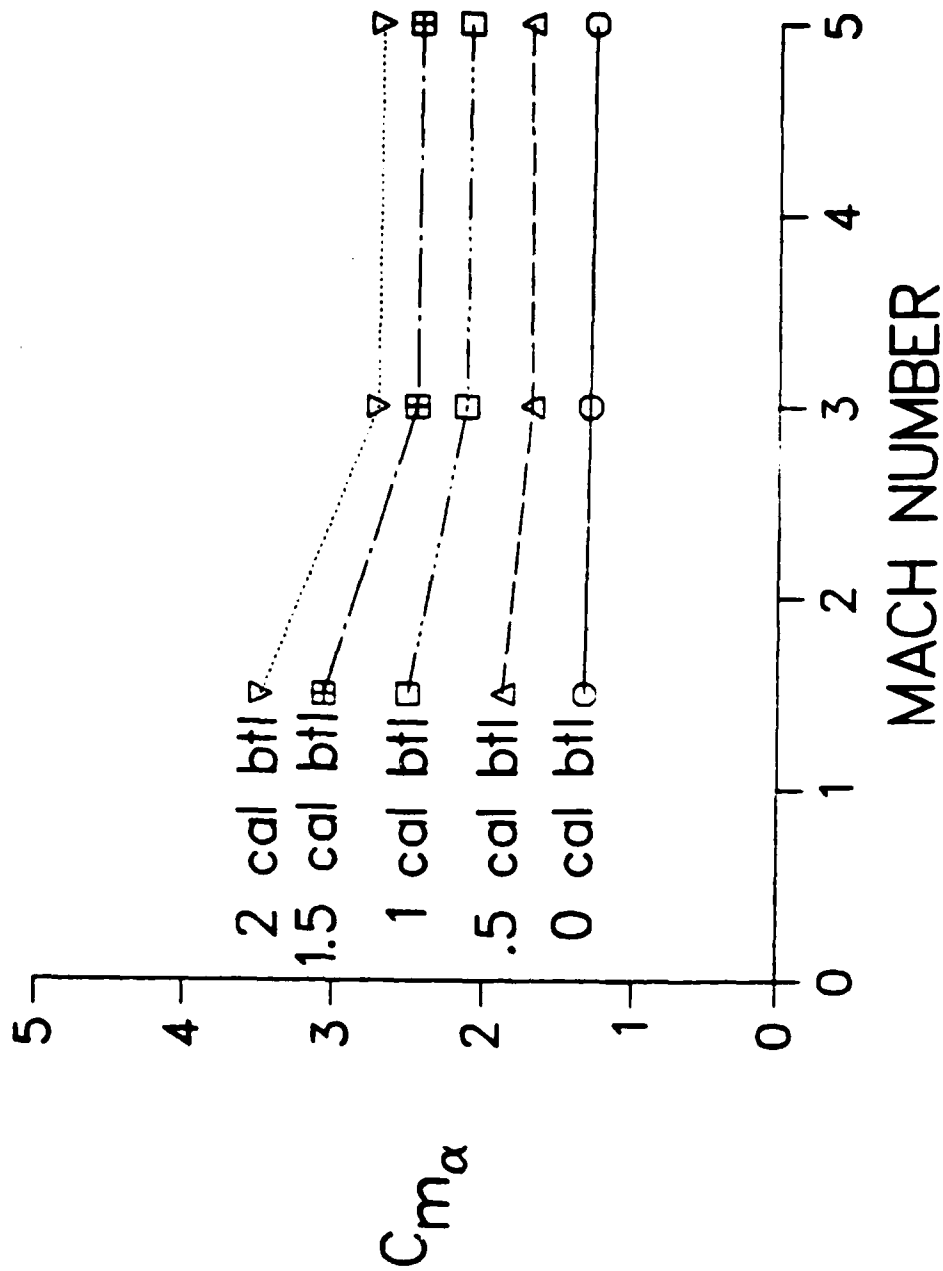


Figure 14. Linear pitching moment coefficient for non-axisymmetric configurations with different boattail lengths.

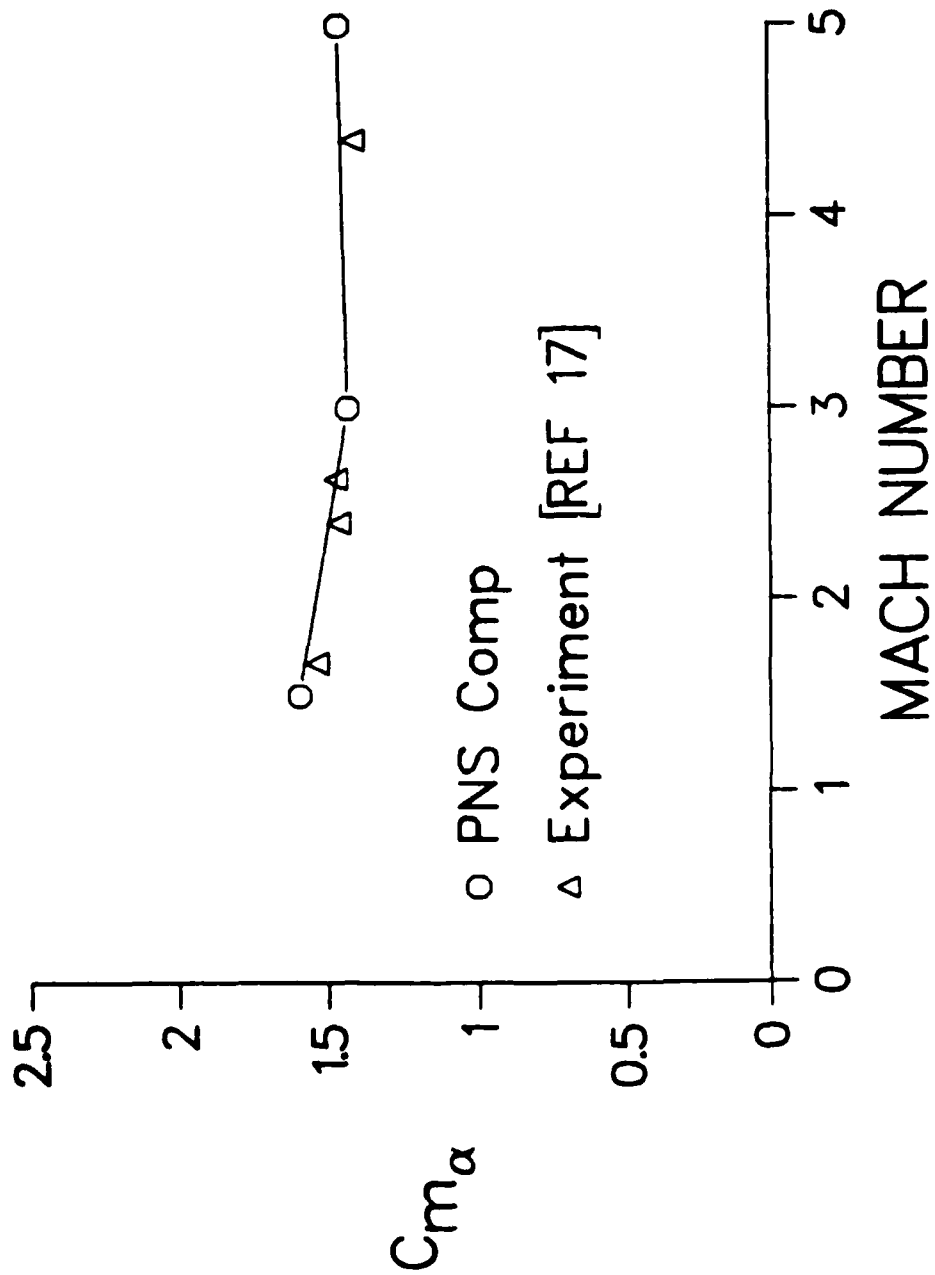


Figure 15. Linear pitching moment coefficient for 1/2 caliber non-conical boattail configuration with small base cavity; comparison between computation and experiment.

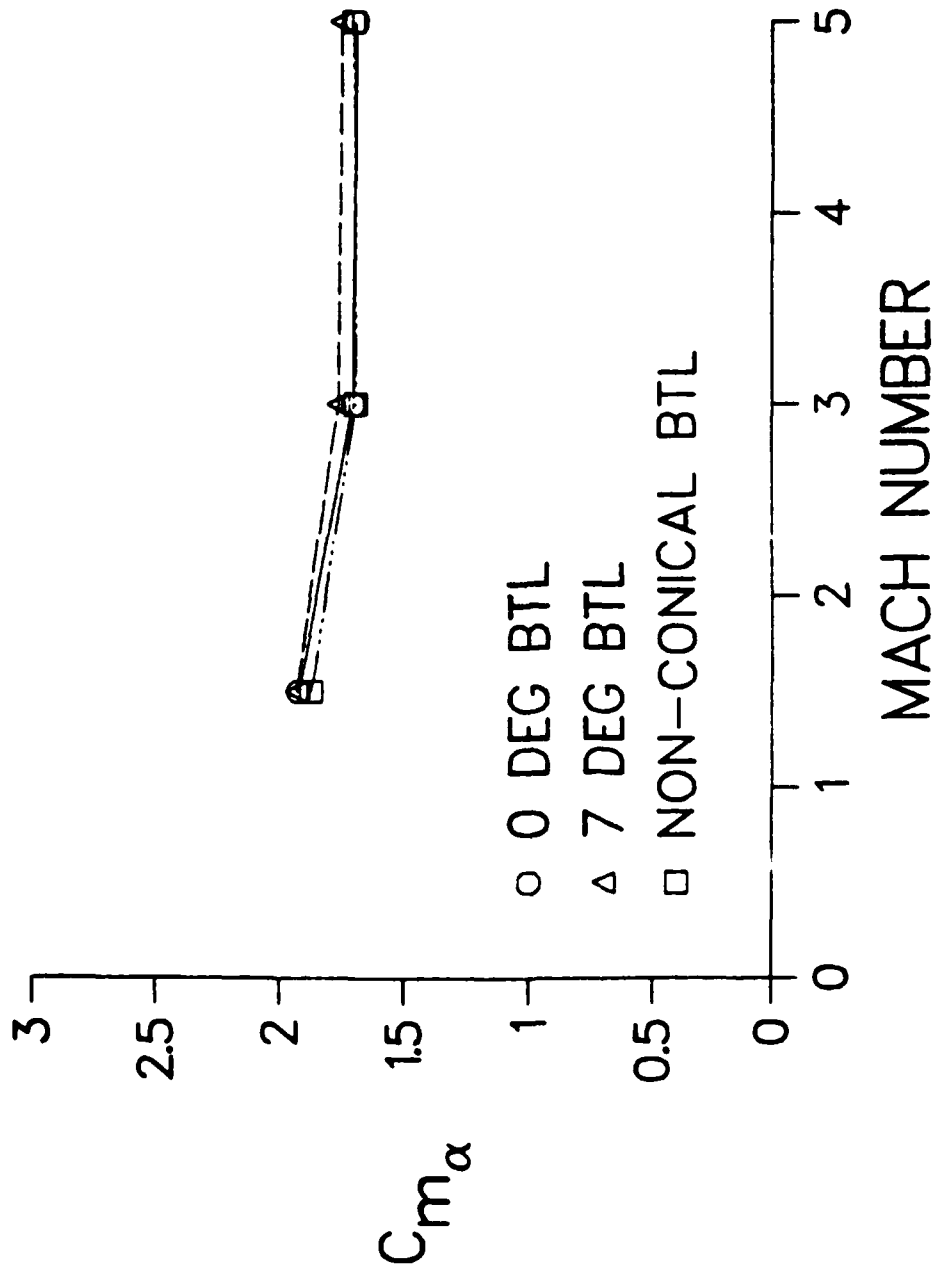


Figure 16. Linear pitching moment coefficient for axisymmetric and non-axisymmetric configurations with 1/2 caliber boattail.

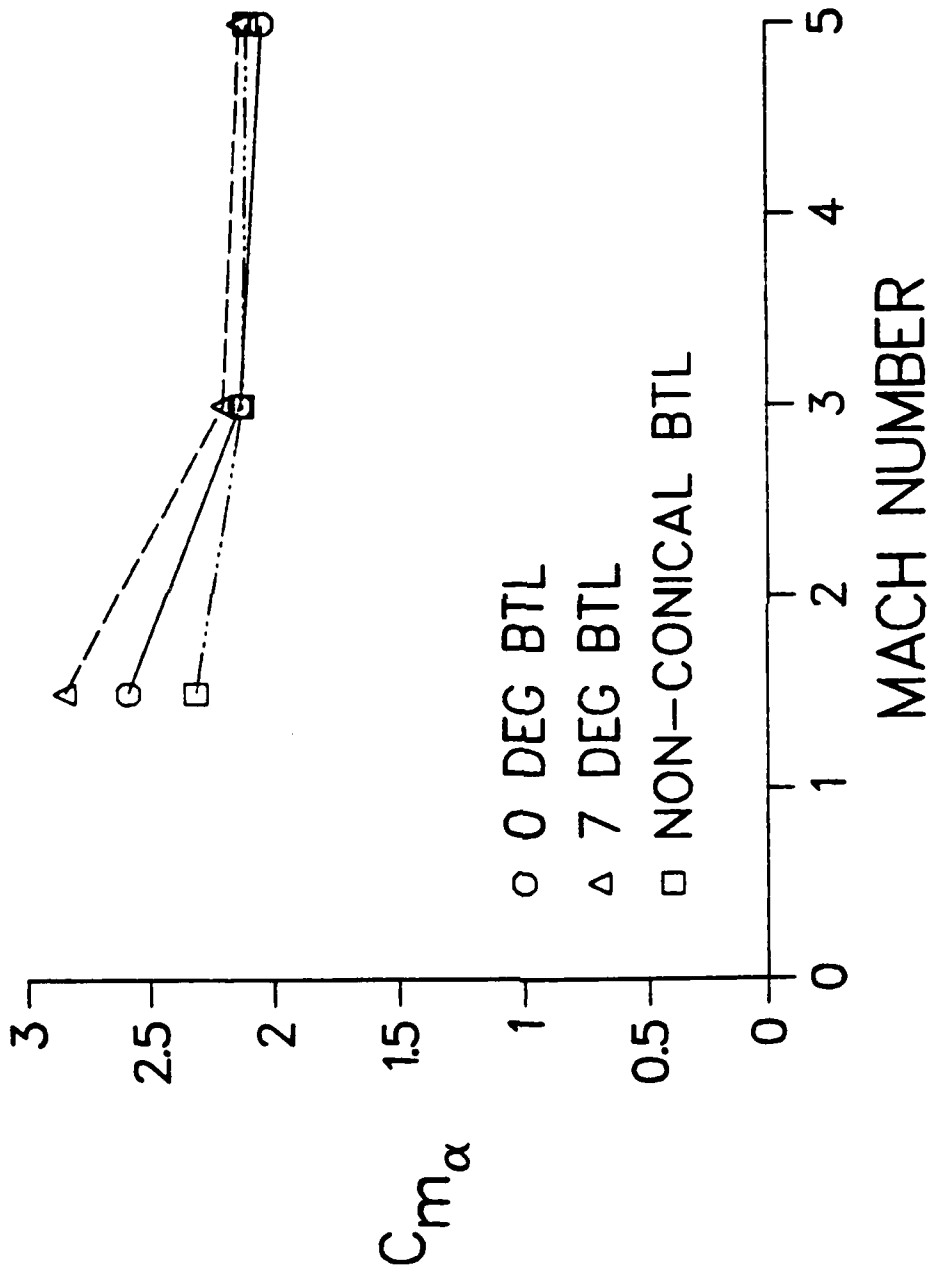


Figure 17. Linear pitching moment coefficient for axisymmetric and non-axisymmetric configurations with 1 caliber boattail.

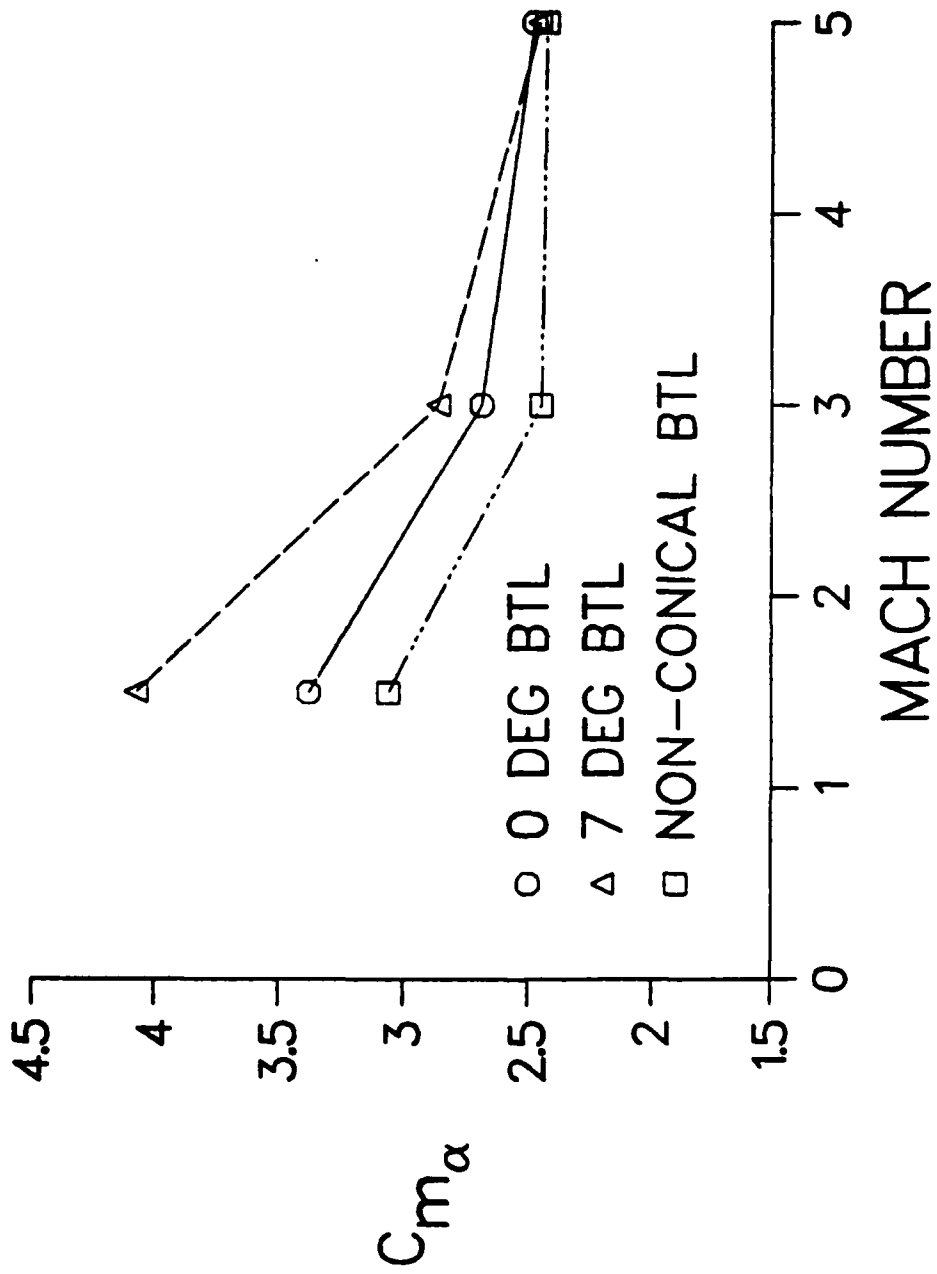


Figure 18. Linear pitching moment coefficient for axisymmetric and non-axisymmetric configurations with 1-1/2 caliber boattail.

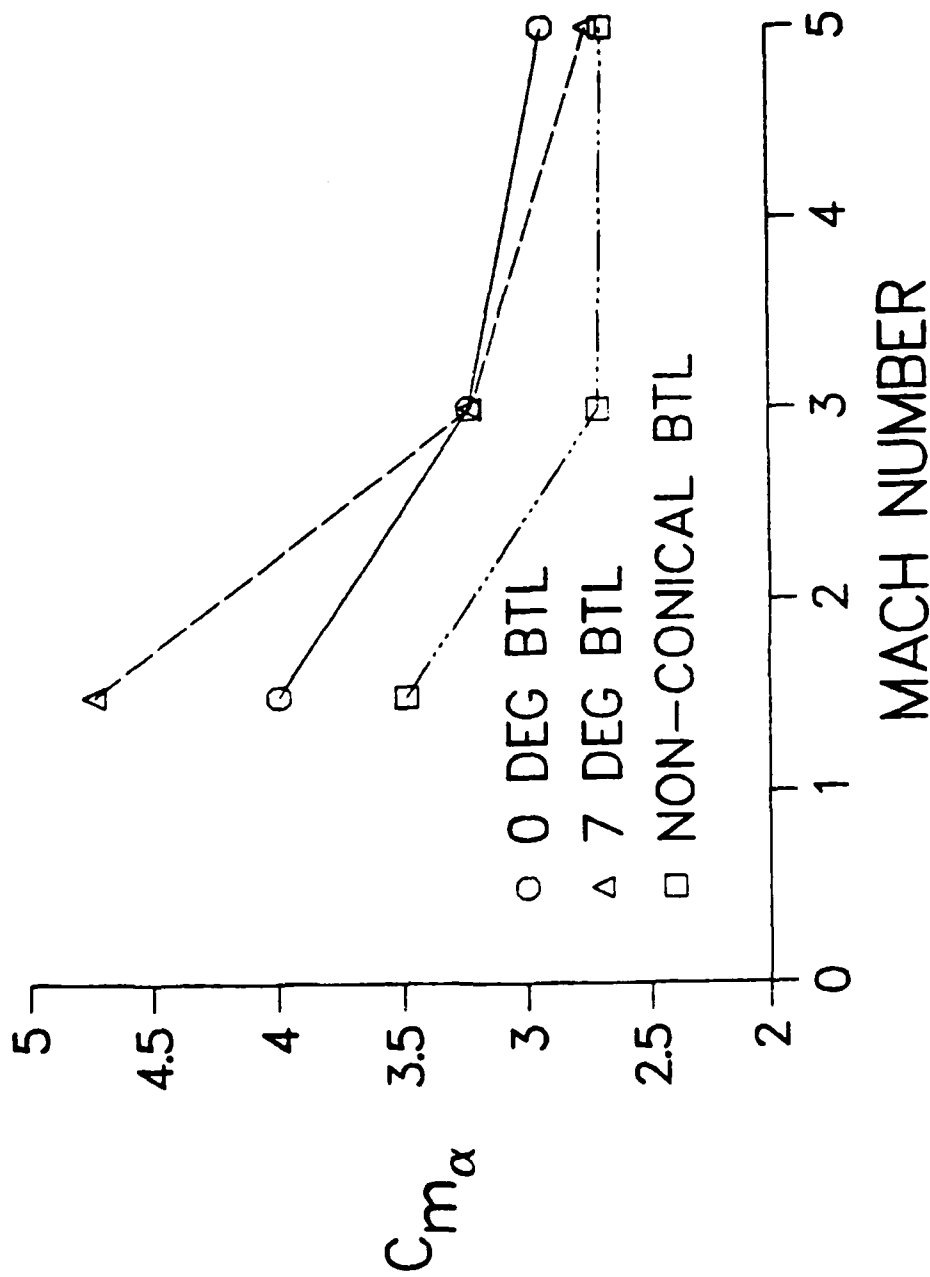


Figure 19. Linear pitching moment coefficient for axisymmetric and non-axisymmetric configurations with 2 caliber boattail.

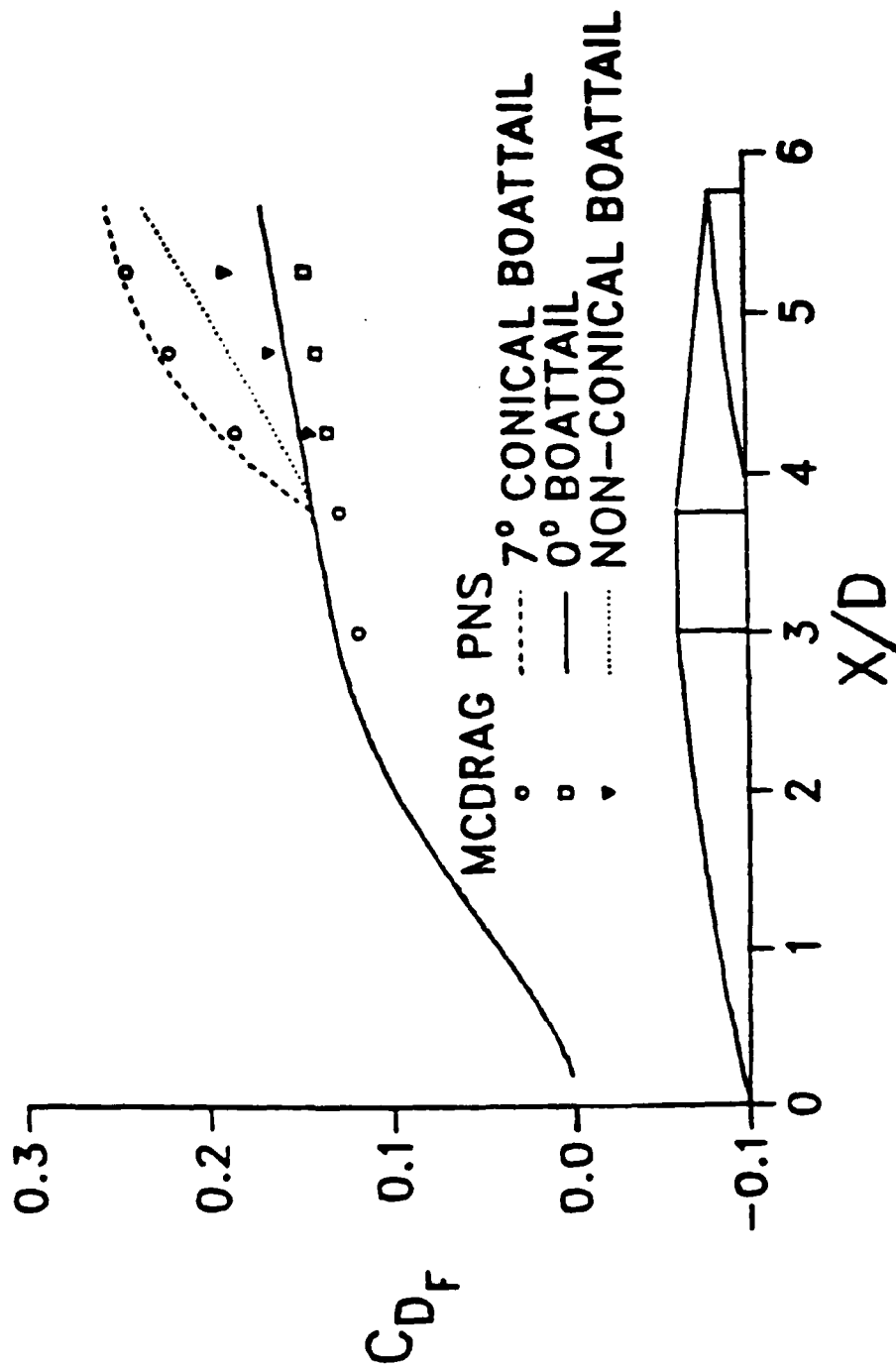


Figure 20. Forebody drag coefficient developing over body, Mach = 1.5, $\alpha = 0^\circ$, axisymmetric and non-axisymmetric configurations.

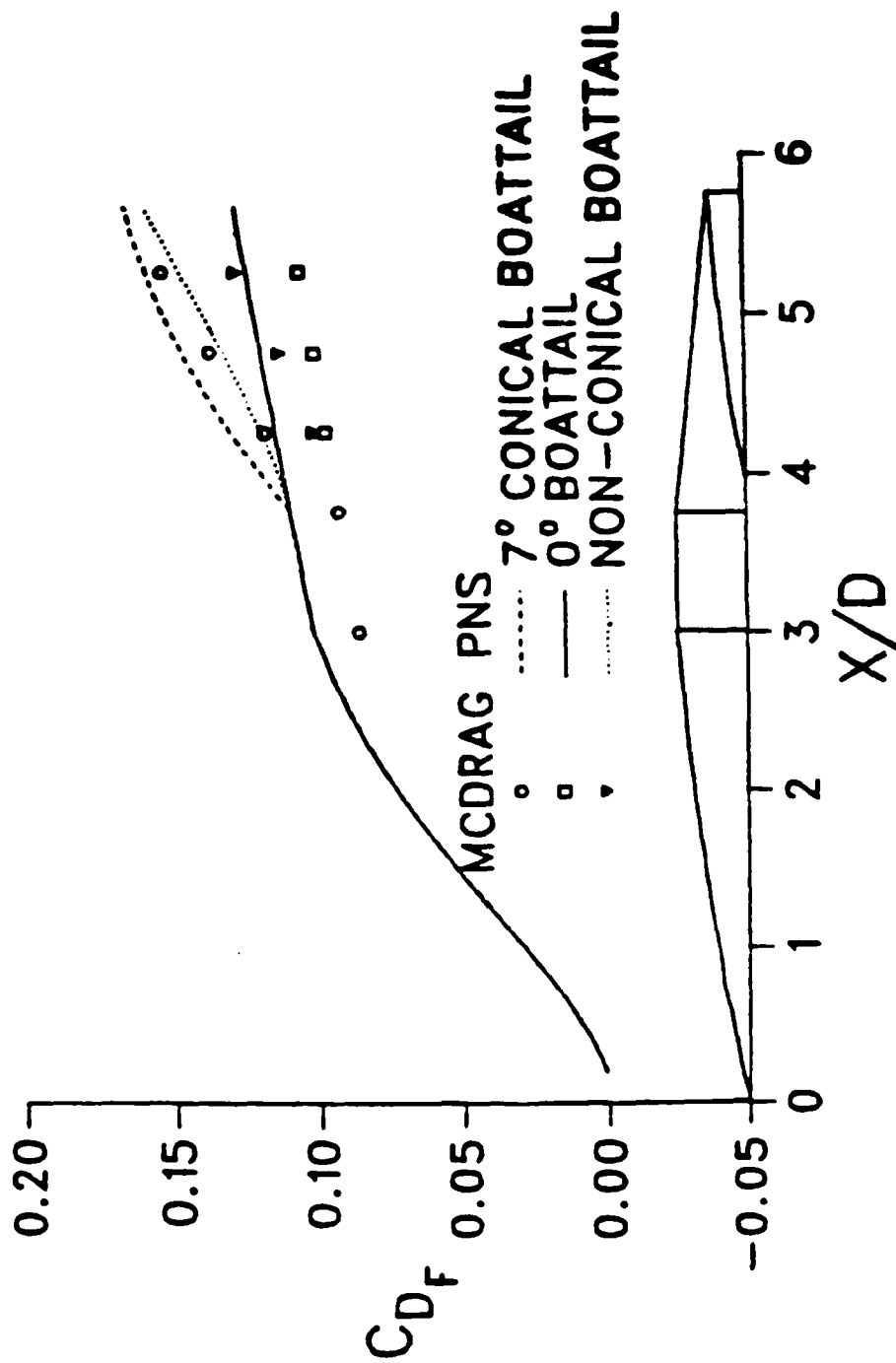


Figure 21. Forebody drag coefficient developing over body, Mach = 3, $\alpha = 0^\circ$, axisymmetric and non-axisymmetric configurations.

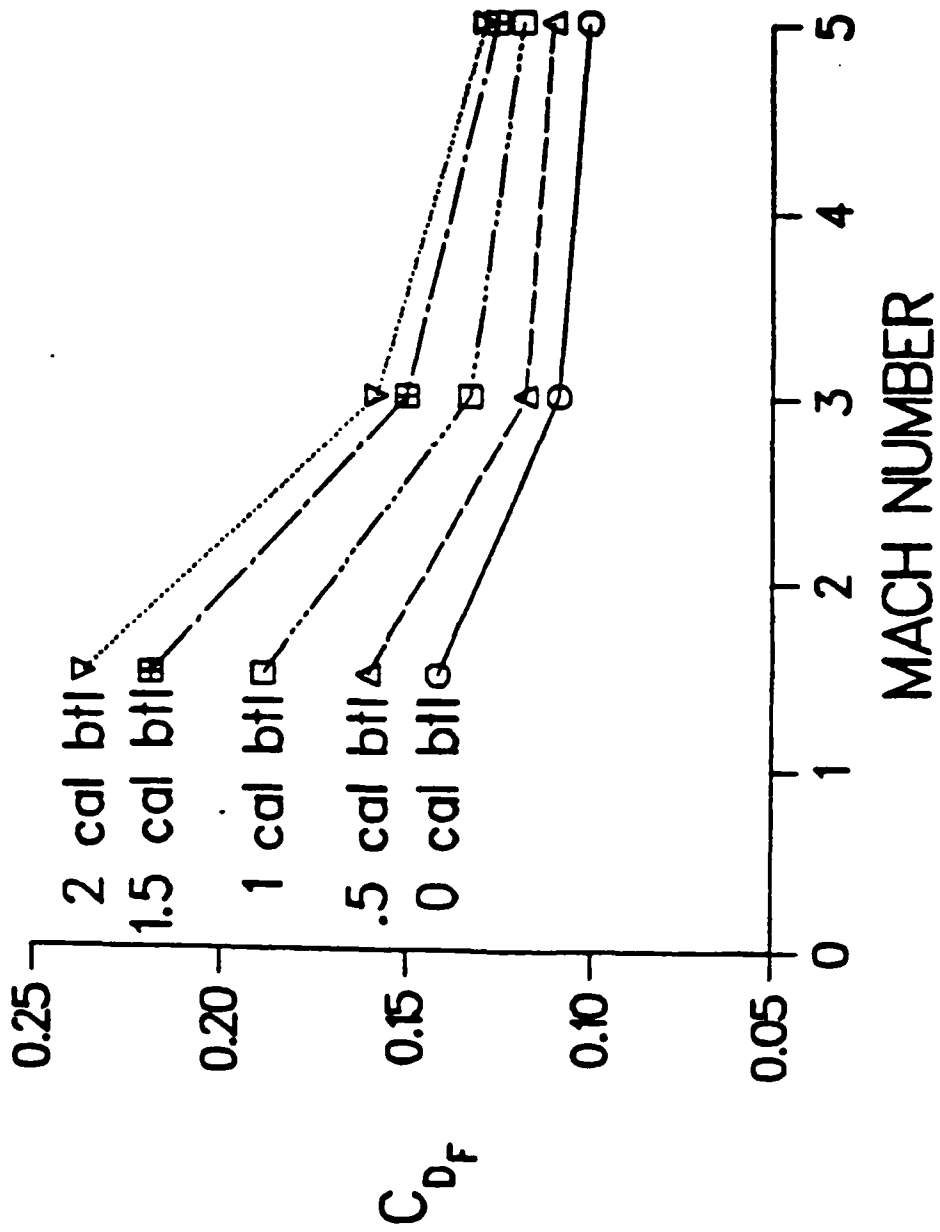


Figure 22. Forebody drag coefficient for non-axisymmetric configuration with different boattail lengths, $\alpha = 0^\circ$.

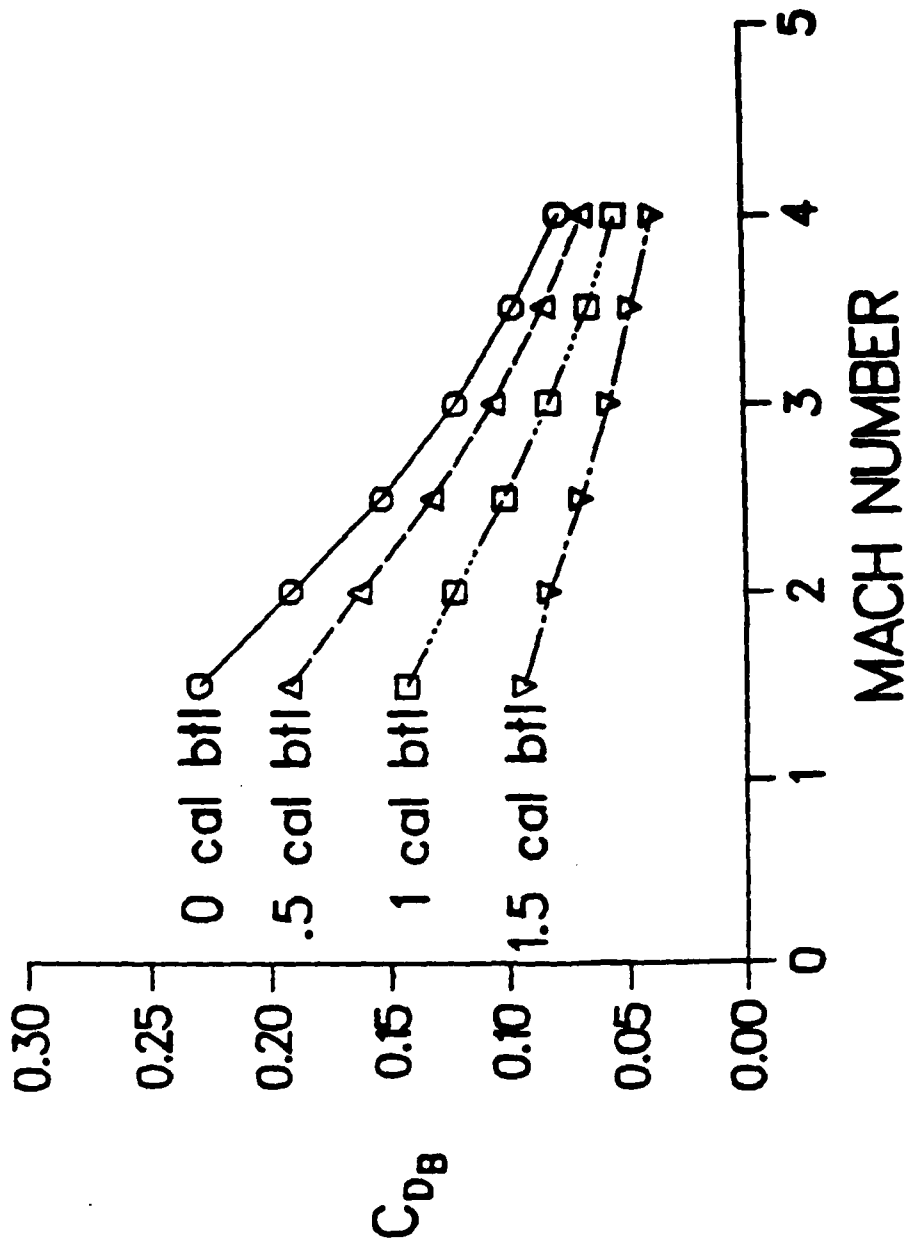


Figure 23. Base drag coefficient for non-axisymmetric configuration with different boattail lengths, $\alpha = 0^\circ$.

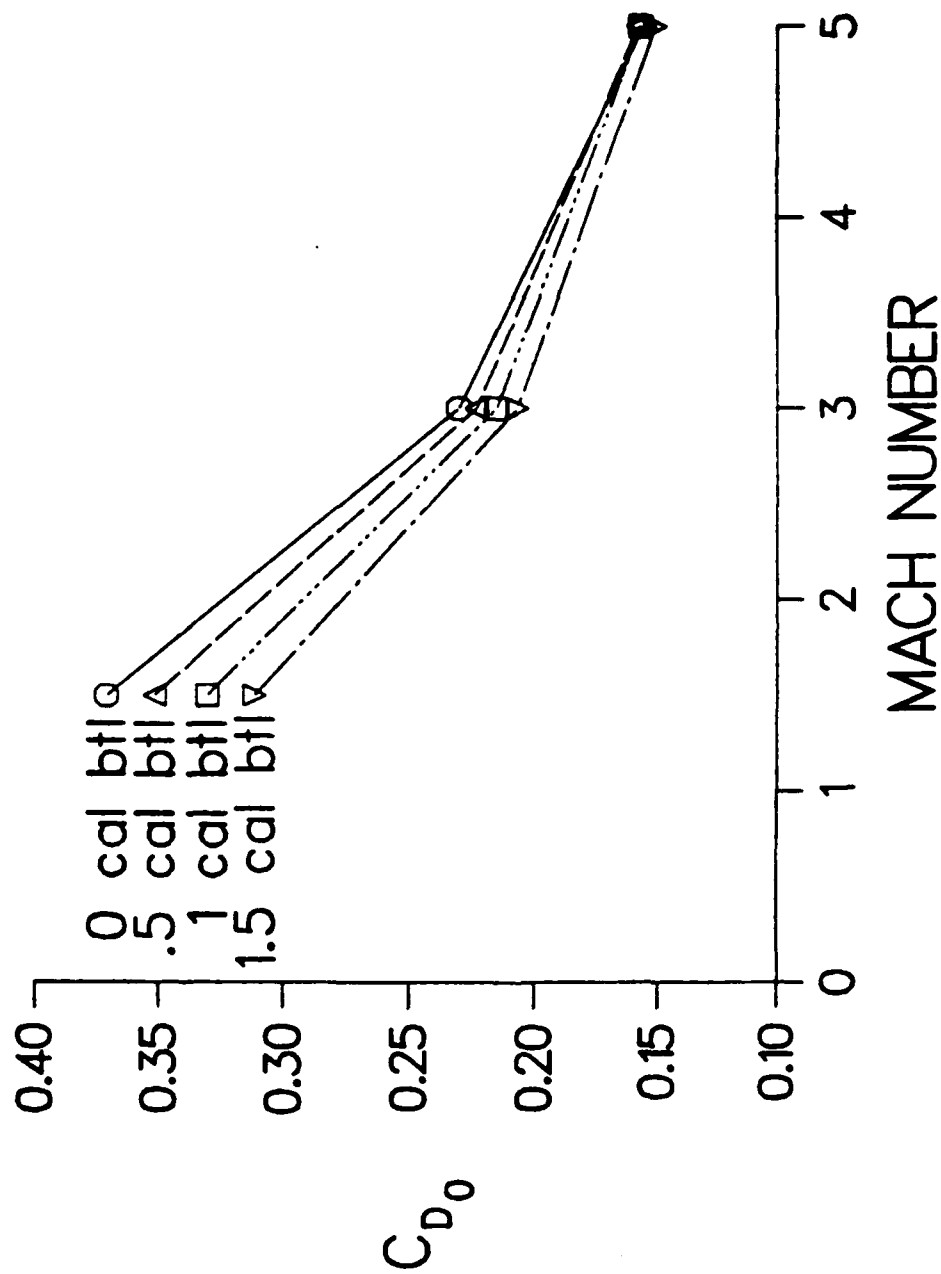


Figure 24. Total drag coefficient for non-axisymmetric configuration with different boattail lengths, $\alpha = 0^\circ$.

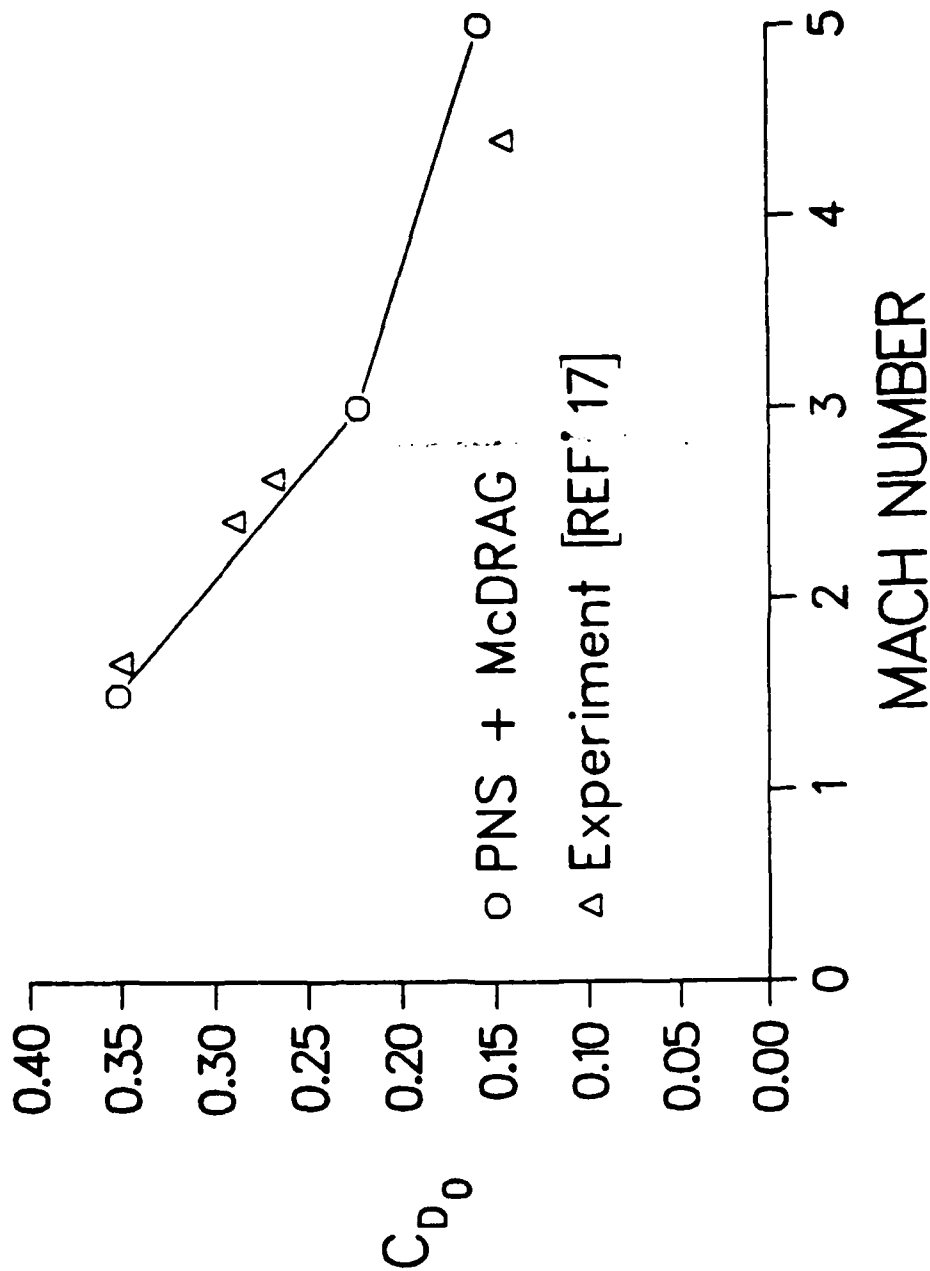


Figure 25. Total drag coefficient for 1/2 caliber non-conical boattail configuration; comparison between computation and experiment.

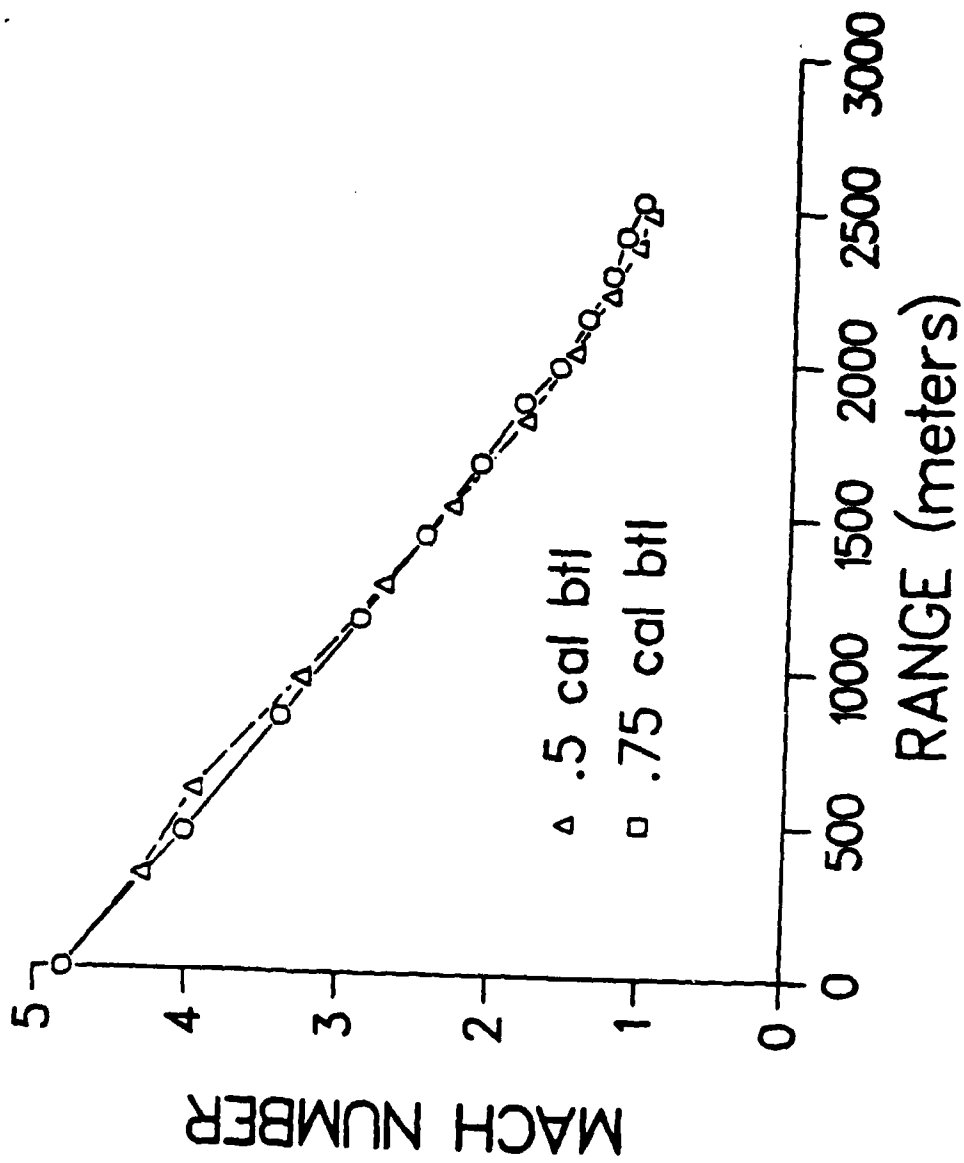


Figure 26. Trajectory simulation for non-axisymmetric configurations, Mach number as a function of range.

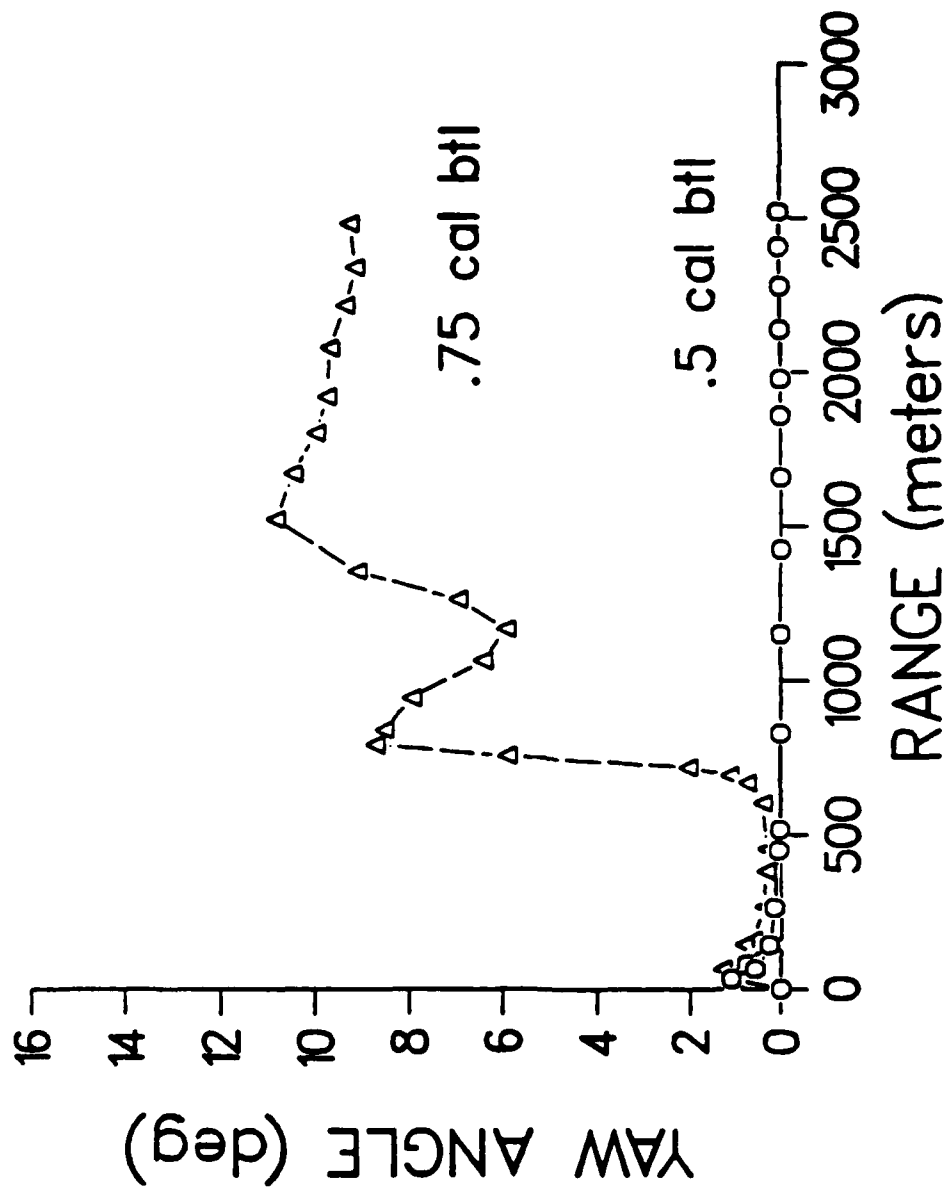


Figure 27. Trajectory simulation for non-axisymmetric configurations; yaw angle as a function of range.

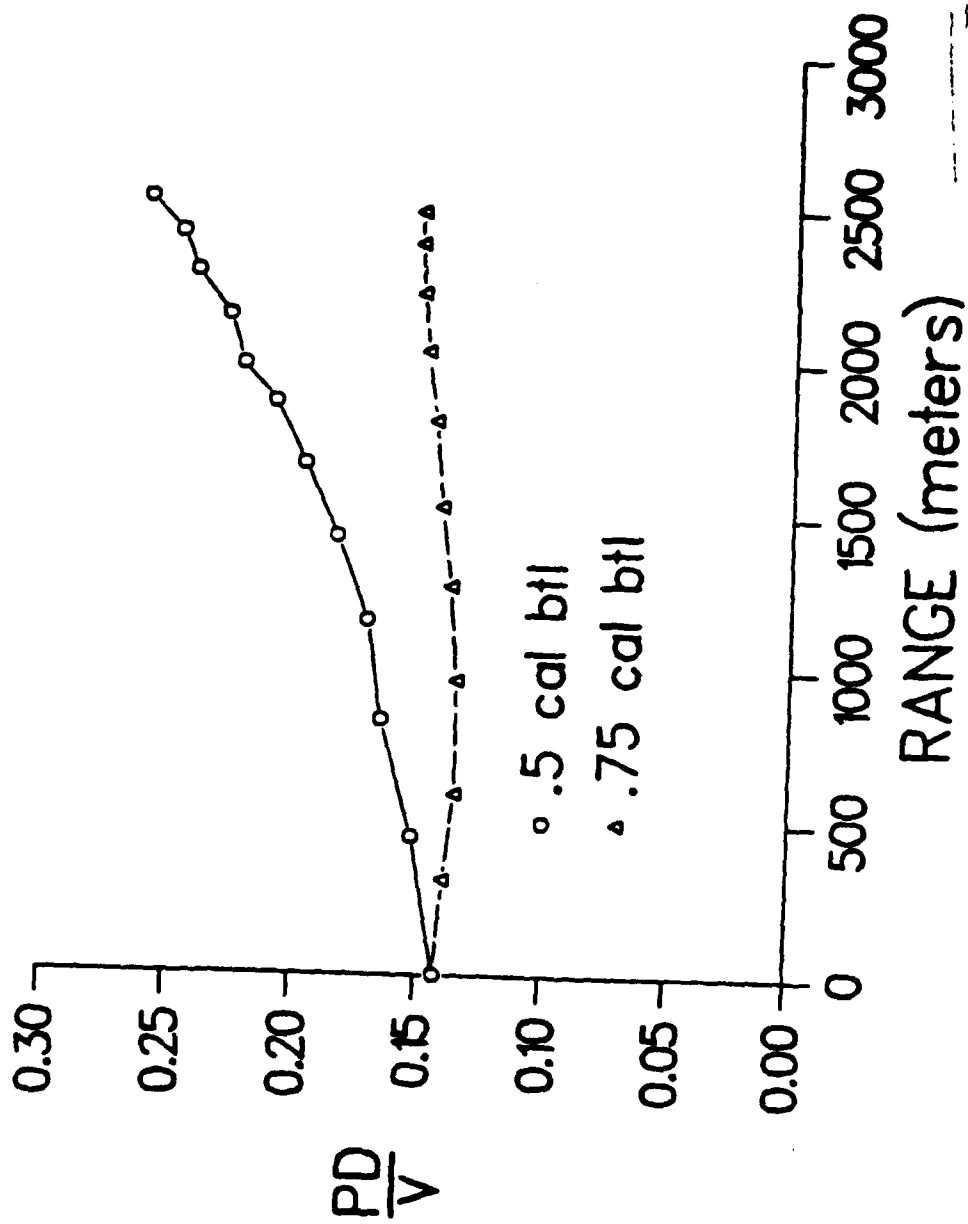


Figure 28. Trajectory simulation for non-axisymmetric configurations; nondimensional spin rate as a function of range.

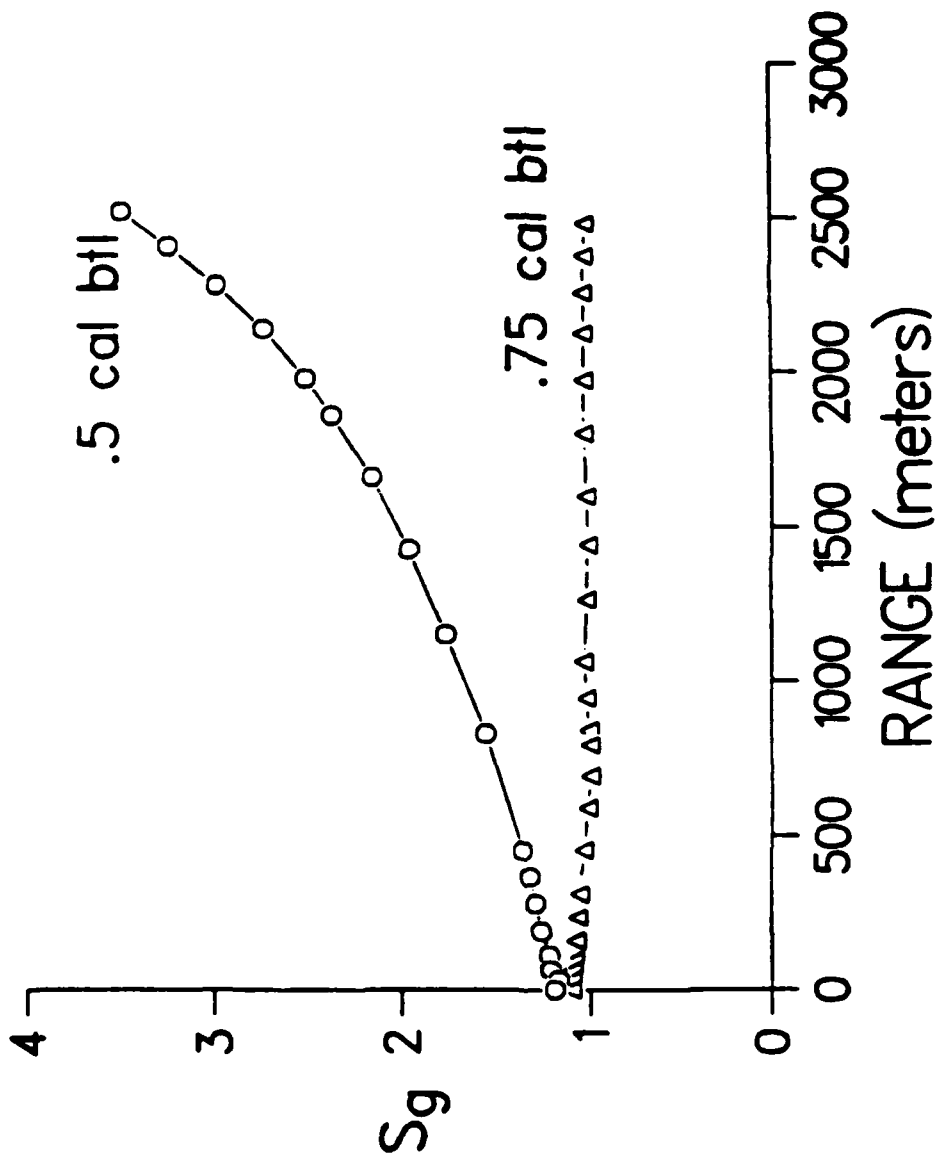


Figure 29. Trajectory simulation for non-axisymmetric configurations; gyroscopic stability as a function of range.

REFERENCES

1. Kayser, L.D. and Sturek, W.B., "Aerodynamic Performance of Projectiles with Axisymmetric and Non-Axisymmetric Boattails," U.S. Army Ballistic Research Laboratory, Aberdeen Proving Ground, Maryland, ARBRL-MR-03022, May 1980. (AD A086091)
2. Kayser, L.D., "Wind Tunnel Tests on a Non-axisymmetric Projectile Shape at Mach Numbers 2.5 to 6.0," U.S. Army Ballistic Research Laboratory, Aberdeen Proving Ground, Maryland, ARBRL-MR-03308, September 1983. (AD A135784)
3. Schiff, L.B. and Steger, J.L., "Numerical Simulation of Steady Supersonic Flow," AIAA Journal, Vol. 18, No. 12, December 1980, pp. 1421-1430.
4. Sturek, W.B. and Schiff, L.B., "Computations of the Magnus Effect for Slender Bodies in Supersonic Flow," U.S. Army Ballistic Research Laboratory, Aberdeen Proving Ground, Maryland, ARBRL-TR-02384, December 1981. (AD A110016)
5. Sturek, W.B., Mylin, W.C., Guidos, B.J. and Nietubicz, C.J., "Navier-Stokes Computational Study of the Influence of Shell Geometry on the Magnus Effect at Supersonic Speeds," U.S. Army Ballistic Research Laboratory, Aberdeen Proving Ground, Maryland, ARBRL-TR-02501, June 1983. (AD A130630)
6. Weinacht, P., Guidos, B.J. and Sturek, W.B., "PNS Computations for Spinning and Fin-Stabilized Projectiles at Supersonic Velocities," U.S. Army Ballistic Research Laboratory, Aberdeen Proving Ground, Maryland, ARBRL-MR-3464, September 1985.
7. Jettmar, R.U. and Kordulla, W., "Computation of Aerodynamic Forces on Bodies with Non-Circular Cross-Section in Supersonic Viscous Flow," AIAA Paper No. 83-2077, AIAA Atmospheric Flight Mechanics Conference, August 1983.
8. Baldwin, B.S. and Lomax, H., "Thin Layer Approximation and Algebraic Model for Separated Turbulent Flows," AIAA Paper No. 78-0257, AIAA 16th Aerospace Sciences Meeting, January 1978.
9. Beam, R. and Warming, R.F., "An Implicit Factored Scheme for the Compressible Navier-Stokes Equations," AIAA Journal, Volume 16, No.4, 1978, pp. 85-129.
10. Rai, M.M. and Chaussee, D.S., "New Implicit Boundary Procedures: Theory and Applications," AIAA Paper No. 83-0123, AIAA 21st Aerospace Sciences Meeting, January 1983.
11. Murphy, C.H., "Free Flight Motion of Symmetric Missiles," U.S. Army Ballistic Research Laboratory, Aberdeen Proving Ground, Maryland, Report No. 1216, July 1963. (AD A442757)

REFERENCES (Continued)

12. Platou, A.S., "An Improved Projectile Boattail," U.S. Army Ballistic Research Laboratory, Aberdeen Proving Ground, Maryland, BRL-MR-2395, July 1974. (AD 785520)
13. Platou, A.S., "An Improved Projectile Boattail, Part II.," U.S. Army Ballistic Research Laboratory, Aberdeen Proving Ground, Maryland, BRL-MR-1866, March 1976. (AD 823839)
14. LaBerge, J.G., "Roll-Oscillation Tests at Subsonic and Supersonic Speeds on a Non-Conical Boattail Missile," National Aeronautical Establishment, Ottawa, Canada, Report LTR-UA-67, April 1983.
15. Maple, C.G., and Synge, J.L., "Aerodynamic Symmetry of Projectiles," Quarterly of Applied Mathematics, Volume IV, pp. 345-366, January 1949.
16. McCoy, R.L., " 'MC DRAG' - A Computer Program for Estimating the Drag Coefficients of Projectiles," U.S. Army Ballistic Research Laboratory, Aberdeen Proving Ground, Maryland, ARBRL-TR-02293, February 1981. (AD A098110)
17. McCoy, R.L. private communication concerning unpublished range data, US Army Ballistic Research Laboratory, Aberdeen Proving Ground, Maryland, September 1986.
18. Lieske, R.F. and McCoy, R.L., "Equations of Motion of a Rigid Projectile," U.S. Army Ballistic Research Laboratory, Aberdeen Proving Ground, Maryland, BRL R 1244, March 1964. (AD 441598)
19. Platou, A.S., "The Influence of the Magnus Moment on the Dynamic Stability of a Projectile," U.S. Army Ballistic Research Laboratory, Aberdeen Proving Ground, Maryland, ARBRL-MR-2155, January 1972. (AD 738016)
20. Plostins, P., private communication concerning launch conditions, US Army Ballistic Research Laboratory, Aberdeen Proving Ground, Maryland, January 1986.

LIST OF SYMBOLS

A	= amplitude of C_{l_α} with respect to roll orientation
a	= speed of sound
C_{D0}	= total drag coefficient at $\alpha = 0^\circ$
C_{DB}	= pressure drag coefficient due to projectile base
C_{DBT}	= pressure drag coefficient due to projectile boattail
C_{DF}	= drag coefficient due to projectile forebody
C_{DH}	= pressure drag coefficient due to projectile head (nose)
C_{DSF}	= skin friction drag coefficient due to entire projectile wetted surface
C_l	= rolling moment coefficient
C_{l_α}	= slope of rolling moment coefficient due to angle of attack and roll orientation
C_{l_p}	= $\partial C_l / \partial (PD/V)$, roll damping coefficient
C_{l_δ}	= $\partial C_l / \partial (\delta_f)$ slope of roll moment coefficient due to canted or deflected lifting surfaces
C_{m_α}	= linear pitching moment coefficient
$C_{m_{\alpha^3}}$	= cubic pitching moment coefficient
$C_{m_q} + C_{m_{\dot{\alpha}}}$	= pitch damping coefficient
C_{N_α}	= $dC_N/d\alpha$, zero- α slope of normal force coefficient
CP	= center of pressure of normal force coefficient
D	= diameter of model
e	= total energy per unit volume of fluid, normalized by $\rho_\infty a_\infty^2$

LIST OF SYMBOLS (Continued)

$\hat{E}_s, \hat{F}, \hat{G}$	= flux vectors of transformed gasdynamic equations
I_x	= axial moment of inertia
I_y	= transverse moment of inertia
M	= Mach number
N	= twist (spin) of model in calibers per revolution
n	= number of fins
P	= spin rate about model axis in rad/sec relative to cross-flow
PD/V	= non-dimensional spin rate about model axis
p	= pressure normalized by $\rho_\infty a_\infty^2$
P_s	= subsonic sublayer pressure
\bar{q}	= vector of dependent variables
\hat{Re}	= Reynold's number, $\rho_\infty a_\infty D / \mu_\infty$
r	= local distance from model axis to body surface
S_g	= gyroscopic stability factor (unconditionally unstable if $S_g < 1$)
\hat{S}	= viscous flux vector
u, v, w	= Cartesian velocity components along x,y,z axes, respectively, normalized by a_∞ .
V	= free stream velocity
x, y, z	= physical Cartesian coordinates
y^+	= distance from wall in law of the wall coordinates
α	= angle of attack
β	= angle of sideslip
δ	= angle of yaw, $\left \sqrt{\alpha^2 + \beta^2} \right $
δ_f	= angle of fin deflection or cant

LIST OF SYMBOLS (Continued)

- ξ, η, ζ = computational coordinates in the axial, circumferential, and radial directions
- θ = roll orientation of shell relative to cross-flow
- μ = coefficient of viscosity, normalized by free stream value
- ρ = density, normalized by free stream value
- ϕ = roll angle; circumferential position on the body measured from windward side
- ω = spin rate about model axis in rad/sec

Subscripts

- ∞ = free stream conditions
- s = sonic layer
- w = body surface value

Superscripts

- T = transpose

DISTRIBUTION LIST

<u>No. of Copies</u>	<u>Organization</u>	<u>No. of Copies</u>	<u>Organization</u>
12	Administrator Defense Technical Info Center ATTN: DTIC-FDAC Cameron Station, Bldg 5 Alexandria, VA 22304-6145	1	Commander US Army Armament, Munitions & Chemical Command ATTN: SMCAR-IMP-L Rock Island, IL 61299-7300
1	HQDA DAMA-ART-M Washington, DC 20310	1	Commander US Army Aviation Systems Cmd ATTN: AMSAV-E 4300 Goodfellow Blvd St. Louis, MO 63120-1798
1	Commander US Army Materiel Command ATTN: AMCDRA-ST 5001 Eisenhower Avenue Alexandria, VA 22333-0001	1	Director US Army Aviation Research & Technology Activity Ames Research Center Moffett Field, CA 94035-1099
10	Commander US Army Armament, Munitions & Chemical Command ATTN: SMCAR-MSI SMCAR-LCA-F/Mertz Loeb Kline Fleming Kahn Hudgins SMCAR-CCL-CA/Hirlinger O'Niell Miller Dover, NJ 07801-5001	1	Commander CECOM R&D Technical Library ATTN: AMSEL-IM-L Ft. Monmouth, NJ 07703-5000
1	Commander US Army Armament, Research, Development & Engineering Cmd ATTN: SMCAR-TDC Dover, NJ 07801	3	Commander US Army Missile Command ATTN: AMSMI-RX Redstone Arsenal, AL 35898-5249
1	Commander US Army Armament, Munitions & Chemical Command ATTN: AMSMC-LEP-L Rock Island, IL 61299	1	Director US Army Missile & Space Intelligence Center ATTN: AIAMS-YDL Redstone Arsenal, AL 35898-5000
1	Commander US AMCCOM ARDEC CCAC Benet Weapons Laboratory ATTN: SMCAR-CCB-TL Watervliet, NY 12189-4050	1	Commander US Army Tank Automotive Command ATTN: AMSTA-TSL Warren, MI 48397-5000
1	Commander US AMCCOM ARDEC CCAC Benet Weapons Laboratory ATTN: SMCAR-CCB-TL Watervliet, NY 12189-4050	1	Director US Army TRADOC Analysis Center ATTN: ATOR-TSL White Sands Missile Range, NM 88002-5502
1	Commander US AMCCOM ARDEC CCAC Benet Weapons Laboratory ATTN: SMCAR-CCB-TL Watervliet, NY 12189-4050	1	Commander US Army Jefferson Proving Ground ATTN: Arthur B. Alphin, MAJ, ARM Madison, IN 47250-5100

DISTRIBUTION LIST

<u>No. of Copies</u>	<u>Organization</u>	<u>No. of Copies</u>	<u>Organization</u>
1	Commander US Army Research Office P.O. Box 12211 Research Triangle Park, NC 27709	1	AFATL/DOIL (Tech Info Ctr) Eglin AFB, FL 32542-5438
1	Commander US Naval Air Systems Command ATTN: AIR-604 Washington, DC 20360	3	Sandia Laboratories ATTN: Dr. W.L. Oberkampf Dr. F. Blottner Division 1636 Albuquerque, NM 87185
2	Commander David W. Taylor Naval Ship ATTN: Dr. S. de los Santos Mr. Stanley Gottlieb Bethesda, MD 20084-5000	3	Director NASA Ames Research Center ATTN: MS-202-1, Dr. T. Pulliam MS-258-1, Dr. J. Steger Dr. L. Schiff Dr. U. Jettmar Moffett Field, CA 94035
2	Commander US Naval Surface Weapons Center ATTN: Code DK20/Clare Moore Dahlgren, VA 22448-5000	1	Massachusetts Institute of Technology ATTN: Tech Library 77 Massachusetts Avenue Cambridge, MA 02139
1	Commander US Naval Weapons Center ATTN: Code 3431/Tech Lib China Lake, CA 93555	1	Virginia Polytechnic Institute & State University P.O. Box 50 Blacksburg, VA 24061
1	Commander US Army Development & Employment Agency ATTN: MODE-ORO Ft. Lewis, WA 98433-5000	1	University of Delaware Mechanical and Aerospace Engineering Department ATTN: K.L. Palko Newark, DE 19711
1	Director NASA Langley Research Center ATTN: NS-185/Tech Lib Hampton, VA 23365	1	Commandant USAFAS ATTN: ATSF-TSM-CN Ft. Sill, OK 73503-5600
2	Commandant US Army Infantry School ATTN: ATSH-CD-CS-OR Ft. Benning, GA 31905-5400	10	CIA OIR/DB/Standard GE47 HQS Washington, DC 20505
1	AFWL/SUL Kirtland AFB, NM 87117-6008	2	Aerojet Ordnance Company ATTN: Jim Parkinson Saul Wasserman 2521 Michelle Drive Tustin California 92680

DISTRIBUTION LIST

<u>No. of Copies</u>	<u>Organization</u>
2	Ford Aerospace and Communications Corporation Aeronutronic Division ATTN: Charles White Bud Blair Ford Road Newpoint Beach, CA 92658
2	Honeywell Inc. ATTN: Wilford E. Martwick Ken Sundeen 600 Second Street, North East Hopkins, MN 55343

Aberdeen Proving Ground

Dir, USAMSAA
ATTN: AMXSU-D
AMXSU-MP/Cohen

Cdr, USATECOM
ATTN: AMSTE-SI-F

Cdr, CRDEC, AMCCOM,
ATTN: SMCCR-RSP-A
SMCCR-MU
SMCCR-SPS-IL

USER EVALUATION SHEET/CHANGE OF ADDRESS

This Laboratory undertakes a continuing effort to improve the quality of the reports it publishes. Your comments/answers to the items/questions below will aid us in our efforts.

1. BRL Report Number _____ Date of Report _____

2. Date Report Received _____

3. Does this report satisfy a need? (Comment on purpose, related project, or other area of interest for which the report will be used.) _____

4. How specifically, is the report being used? (Information source, design data, procedure, source of ideas, etc.) _____

5. Has the information in this report led to any quantitative savings as far as man-hours or dollars saved, operating costs avoided or efficiencies achieved, etc? If so, please elaborate. _____

6. General Comments. What do you think should be changed to improve future reports? (Indicate changes to organization, technical content, format, etc.) _____

CURRENT ADDRESS _____
Name
_____ Organization
_____ Address
_____ City, State, Zip

7. If indicating a Change of Address or Address Correction, please provide the New or Correct Address in Block 6 above and the Old or Incorrect address below.

OLD ADDRESS _____
Name
_____ Organization
_____ Address
_____ City, State, Zip

(Remove this sheet, fold as indicated, staple or tape closed, and mail.)

FOLD HERE

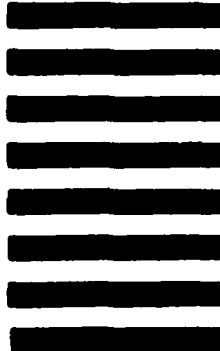
Director
US Army Ballistic Research Laboratory
ATTN: DRXBR-OD-ST
Aberdeen Proving Ground, MD 21005-5066



NO POSTAGE
NECESSARY
IF MAILED
IN THE
UNITED STATES

OFFICIAL BUSINESS
PENALTY FOR PRIVATE USE, \$300

BUSINESS REPLY MAIL
FIRST CLASS PERMIT NO 12062 WASHINGTON, DC
POSTAGE WILL BE PAID BY DEPARTMENT OF THE ARMY



Director
US Army Ballistic Research Laboratory
ATTN: DRXBR-OD-ST
Aberdeen Proving Ground, MD 21005-9989

FOLD HERE

END

11-87

DTIC